REVIEW

Check for updates

Progress in fullerene-based hybrid perovskite solar cells

Edison Castro, [ID] Jesse Murillo, Olivia Fernandez-Delgado [ID] and
Luis Echegoyen [ID] *

In this review, we summarize recent advances that have resulted in fullerene-based high-efficiency perovskite solar cells (PSCs) by new processing methods of the perovskite films, by adding fullerenes as interfacial selective electron extraction layers and improving device stability or by incorporating fullerene derivatives to eliminate hysteretic behavior of both regular and inverted PSC structures. Finally, we outline some perspectives for further advancing PSCs for large-scale and commercial applications.

1. Introduction

Solar energy is one of the most promising alternatives to meet world energy demands.[1,2] In this regard, PSCs have emerged as a very promising new type of photovoltaic technology due to their low-cost, ease of fabrication and high power conversion efficiency (PCE) above 22%, which is higher than that obtained with polycrystalline silicon, while using 1000 times less light harvesting material.[3–8]

Perovskites with general formula ABX_3, where A is a monovalent cation, methylammonium (MA) or formamidinium (FA), B is Pb(II) and X is a halogen (chlorine, bromine or iodide), are the most investigated materials (Fig. 1a and b).[8–10] These perovskite materials exhibit very interesting properties, such as tunable bandgaps, high absorption coefficients, long charge

carrier (electron–hole) diffusion lengths, and low-temperature solution processability.[11–14] The exceptional properties of these materials allow for the fabrication of devices either with the regular n–i–p or the inverted p–i–n configurations (p refers to a p-type semiconductor, n to an n-type semiconductor, and i to an undoped semiconductor).[3,10,15] The latter has recently attracted more attention due to the relatively simple device architecture and low-temperature manufacturing process that make them suitable for commercial applications.[16,17]

Herein, we focus on the recent advances that enable the high photovoltaic performance and long-term stability of PSCs through: processing of the perovskite films, some approaches based on their composition (presence of additives), the use of fullerene derivatives in different device architectures (regular and inverted), and the results of calculations based on the perovskite/fullerene interface. These lead to final considerations to design optimally performing fullerenes. Finally, we outline some perspectives on how to further advance PSCs for large-

Department of Chemistry, University of Texas at El Paso, 500 West University Avenue, El Paso, TX, USA. E-mail: echegoyen@utep.edu

Edison Castro was born in Nariño, Colombia. He obtained his BSc from the Universidad de Nariño, Pasto-Colombia in 2008, his MSc degree from the Universidad del Valle, Cali-Colombia in 2011, and his PhD from The University of Texas at El Paso in 2017, under the supervision of Prof. Luis Echegoyen. His current research interests include the synthesis of fullerene derivatives for photovoltaic and biological applications, and design of perovskite solar cells.
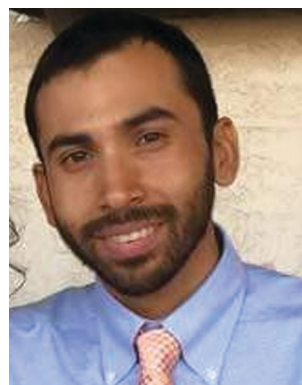
Edison Castro

Jesse Murillo received his BS in Chemistry from the University of Texas at El Paso in 2013. Currently, he is pursuing his PhD in the field of chemistry at the University of Texas at El Paso. He is being co-advised by Prof. Luis Echegoyen and Prof Skye Fortier. His current research interest is in endohedral fullerene synthesis, perovskite crystal growth, and inorganic synthetic chemistry.
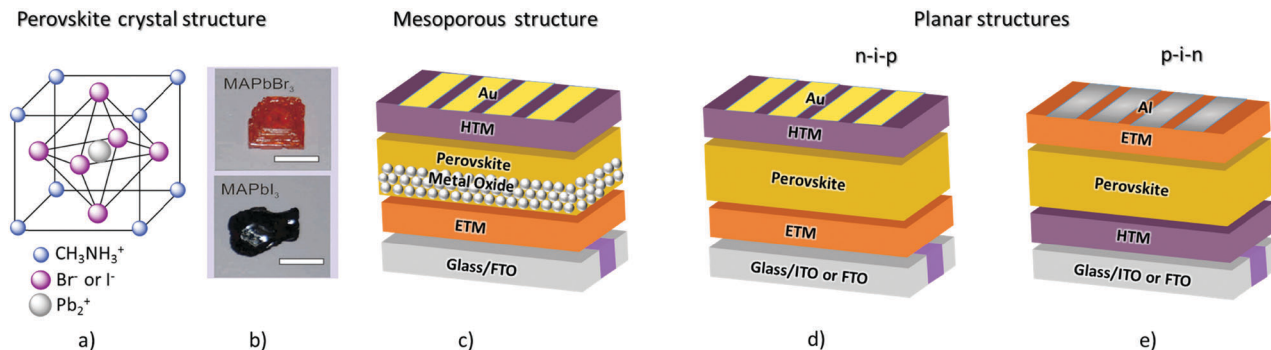
Jesse Murillo

Fig. 1 (a) Three-dimensional crystal structure representation of MAI/MABr perovskite. (b) Images of crystalline MAPbI$_3$ and MAPbBr$_3$ material, scale bars: 5 mm. Adapted with permission from ref. 32. Copyright 2016, Nature Publishing Group. PSCs devices, (c) mesoporous, (d) planar (regular) n−i−p and (e) planar (inverted) p−i−n.

scale and commercial applications. There are other reviews that describe in more detail the different perovskite structures,[2] working principles,[18] photophysics,[19] chemical and thermal stability,[9,20] deposition techniques,[21,22] and comparison with other photovoltaic technologies.[8]

2. Device structures

PSCs have been traditionally fabricated with mesoscopic and planar heterojunction structures (Fig. 1). The mesoscopic structures (Fig. 1c) are composed of fluorinated-doped tin oxide (FTO), a mesoporous metal oxide scaffold that works as an electron transporting material (ETM) such as titanium oxide (TiO$_2$) or aluminum oxide (Al$_2$O$_3$), the perovskite material, which can infiltrate into the mesoporous scaffold or be used as a capping layer on top of the ETM, and a hole transporting material (HTM) such as spiro-OMeTAD, and a metal contact (Ag or Au) electrode.[10] Later, it was found that PSCs can also be fabricated with planar configurations (Fig. 1d and e) for which efficiencies above 20% have been reported.[23–26]

The planar configurations include regular (n−i−p)[25] and inverted (p−i−n)[15] devices. For these devices, the hole and electron transporting layers are crucial because they determine the polarity of the device, improve stability, passivate surface charge traps, and help charge extraction and transport from the active layer to the electrodes.[27–30]

The best performing devices thus far are those based on mesoscopic structures (22.1% PCE).[31] However, it is worth noting that the efficiencies of planar devices have also improved to certified values of 21.04%, and the fabrication of planar devices is relatively easier compared to those of TiO$_2$-based mesoporous devices.[26]

3. Deposition- and solution-processed perovskite thin films

There are many reported procedures to deposit the organic–inorganic perovskite material, each based on the same principle – the reaction of an organic material (MAI or FAI) and an inorganic material (PbI$_2$, PbBr$_2$ or PbCl$_2$) that yield different crystalline and film quality, and different degrees of surface coverage. It has been reported that pin hole free perovskite layers highly improve device performance.[6,19] One area of focus

Olivia Fernandez-Delgado was born in Havana, Cuba. She obtained her BSc from the University of Havana, Cuba in 2016. Currently, she is pursuing her PhD under the supervision of Prof. Luis Echegoyen and Prof. Chu-Young Kim at The University of Texas at El Paso. Her current research interests include the synthesis and characterization of fullerene derivatives for photovoltaic and biological applications, as well as the design of inverted perovskite solar cells.

Olivia Fernandez-Delgado

Prof. Luis Echegoyen obtained both his BSc and PhD from the University of Puerto Rico in Rio Piedras. After several professorships at the Universities of Puerto Rico, Maryland, and Miami he was appointed Chair of the Department of Chemistry at Clemson University, in South Carolina. Later he served as Division Director for Chemistry at the National Science Foundation for 4 years (2006-2010) and more recently, he became the Robert A. Welch Professor of Chemistry at the

Luis Echegoyen

University of Texas-El Paso in 2010. His research interests include fullerene chemistry, electrochemistry, and supramolecular chemistry, with special emphasis in photovoltaics and endohedral fullerenes.

for improving device efficiencies is the optimization of film crystallinity. Two different methodologies have shown high quality, uniform and smooth thin films; vapor deposition and solution processing techniques, see below.

3.1 Vapor-assisted film deposition methods

The vapor-assisted method for perovskite film formation was introduced by Liu et al.[33] who achieved an efficiency of over 15% for planar PSCs (Fig. 2a). In this dual-source method, MAI and PbI_2 are heated at 120 °C and 325 °C, respectively, and deposited on a TiO_2 layer under high vacuum. Using this method, Momblona et al.[34] reported PCEs up to 20% for n–i–p and 16.5% for p–i–n configurations. This technique offers a uniform layer ($\sim$500 nm), grain sizes in the nanometer scale, pin-hole free perovskite films and the ability to prepare multi-stack thin films. A variant of this method is the deposition of the perovskite at low temperature by a vapor-assisted solution process (Fig. 2b). The as-prepared PbI_2 layer is treated with MAI (vapor) under a N_2 atmosphere for 2 h. The perovskite film derived from this approach exhibits full surface coverage, uniform grain structure with grain sizes up to micrometers, and 100% precursor transformation completeness.[35] The vapor-assisted deposition techniques have been reviewed in more detail by Ono et al.[21]

3.2 Solution methods

Despite the good results obtained with the vapor-deposition techniques, most research has been focused on solution methods because they offer more alternatives for preparing perovskite films at relatively low temperatures. The solution methods can be categorized into one-step and two-step Fig. 2c, d and e–g, respectively. Solution deposition methods have been reviewed in more detail by Zhou et al.[22] and Liu et al.[15]

3.2.1 One-step. In this method stoichiometric amounts of the precursors (organo-halide and metal-halide) are mixed to form the perovskite solution,[36] which is spin coated directly onto the substrate followed by an annealing process at 100 to 150 °C (Fig. 2c). High performing devices can be fabricated using different MAI : PbI_2 composition ratios from 1 : 2 to 4 : 1, respectively.[37–39] Lee et al.[40] reported for the first time that devices prepared by the one-step solution method can achieve 10.9% PCE values. Since then, many advanced solvent engineering techniques have been developed and efficiencies above 20% have been achieved.[25,41–43]

The one-step is the simplest technique for preparing perovskite thin films, however the morphological control for the perovskite films based on this method is challenging[44] and the incorporation of additives such as DMSO,[45,46] 1,8-diiodooctane[47] (DIO), HI[48] and HBr[49] to slow down crystal growth to improve the surface morphology of spin-coated perovskite films has been employed (Fig. 2d).

On the contrary, Jeon et al.[50] have reported that the addition of an antisolvent that does not dissolve the perovskite films, such as toluene, on top of the wet perovskite film during spin-coating results in fast crystallization. Thus, a dense perovskite film can form uniformly across the substrate. The addition of other antisolvents such as chlorobenzene, benzene, diethyl ether and xylene have also been reported.[42,51,52]

3.2.2 Two-step. In 2013, Burschka et al.[53] first reported the application of this method for PSCs fabrication and a PCE of 15% was achieved. Typically, in this method a PbI_2 layer is converted into $MAPbI_3$ by dipping the substrate into a MAI solution,[53] spin coating MAI on top of the PbI_2 layer[54] (Fig. 2f and g) or by exposing the PbI_2 film to a MAI vapor atmosphere[35] (Fig. 2b). High quality and more reproducible perovskite films can be prepared using this method. Additionally, varying the
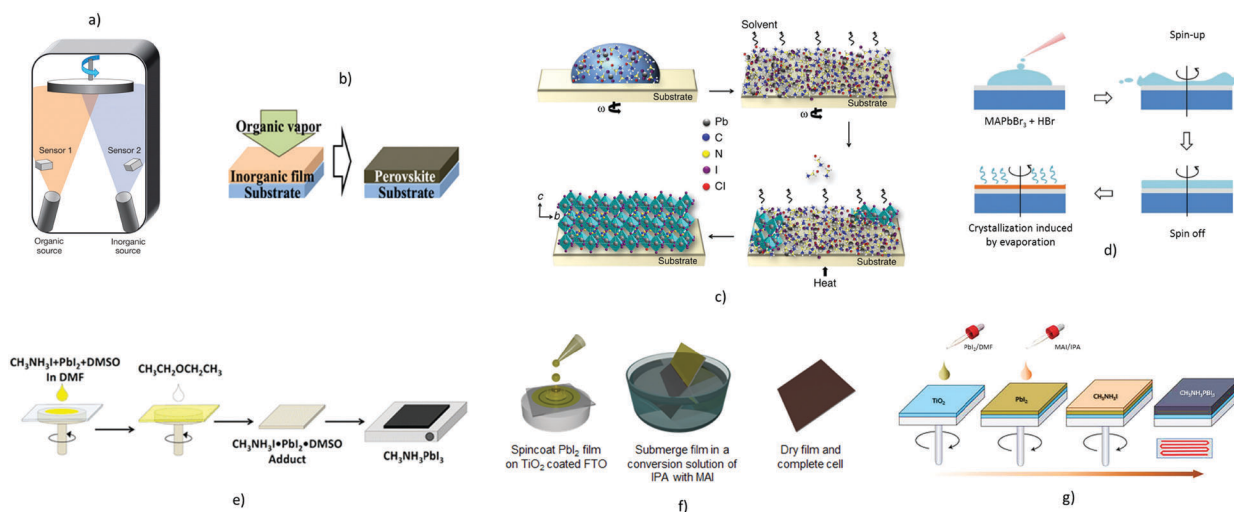

Fig. 2 Different deposition methods for high quality perovskite films. (a) Adapted with permission from ref. 33. Copyright 2013 Nature Publishing Group. (b) Adapted with permission from ref. 58. Copyright 2013 American Chemical Society. (c) Reproduced with permission.[36] Copyright 2015, Nature Publishing Group. (d) Reproduced with permission.[49] Copyright 2016, John Wiley and Sons. (e) Reproduced with permission.[42] Copyright 2016, American Chemical Society. (f) Reproduced with permission.[59] Copyright 2016, American Chemical Society. (g) Reprinted with permission from ref. 54. Copyright 2014, Nature Publishing Group.

concentration of the MAI solution, the perovskite grain sizes can be improved.[54] Using the two-step method, Yang et al.[55] have reported efficiencies exceeding 20%. The addition of additives to control the formation of the perovskite film by this method has also been extensively studied (Fig. 2e).[42,56,57]

4. The use of fullerenes in PSCs

In 2013, fullerene C_{60} (1) and its derivatives phenyl-C_{60}-butyric acid methyl ester ($PC_{61}BM$) (2) and tetrahydro-di[1,4]methano-naphthaleno[5,6]fullerene-C_{60} (3) indene bis adduct (ICBA) (Fig. 3) were introduced into PSCs for the first time by Jeng et al.[60] and PCEs of 3.0, 3.9 and 3.4% were achieved, respectively, when used as ETMs. Recently, Grätzel[24] and co-workers reported efficiencies above 20% for an inverted PSC device with the configuration of ITO/PEDOT:PSS/perovskite/$PC_{71}BM$ (4)/CaAl, whereas a PCE of 18.5% was reported by Huang[61] and coworkers for a PSC device based on a pure ICBA isomer (trans-3) (5) (Fig. 3). It has been widely demonstrated that the use of fullerenes either as ETMs, interface modification of the ETM[1,16,30,62–109] or as additives[43,69,92,110–114] in the perovskite layer can play an important role in passivating the charge traps at the surfaces and grain boundaries of the thin films, which significantly reduces the hysteresis and leads to higher device performances. Additionally, fullerenes can also act as a barrier for moisture, thus enhancing long-term stability and also as a template for perovskite crystal growth and to decrease or even completely avoid ion migration.[115]

In recent years much work has been dedicated to reduce the hysteretic J–V behavior in hybrid perovskite devices. One phenomenon believed to contribute to this behavior is the creation of charge trap states at layer interfaces and crystal grain boundaries within devices. Work done by Wojciechowsk et al.[85] has shown the usefulness of fullerene derivatives in reducing charge trap/de-trapping processes in PSC devices, which contribute significantly to this behavior.

When considering the effect of fullerenes on the performance of a PSCs, electronic properties should not be the only factors examined. Indeed, morphology of the fullerene and the fullerene/surface layer has been shown to be an important parameter for the quality of the PSC characteristics. Some fullerene derivatives can form dimers and polymers in the device layers, rather than discrete molecular species. Huemueller et al.[116] studied the effect of polymeric fullerenes on device efficiencies and stabilities. Their study showed a direct correlation between the amount of polymerized fullerene and J_{sc}/V_{oc} efficiency losses. In addition, the authors reported an annealing method that allows the polymerization of the photoactive layer while still maintaining monomeric crystallinity of the fullerene species. With their proposed process, fullerenes are more evenly dispersed in the polymer layer, thus reducing the likelihood of fullerene to fullerene exciton driven dimerization. Along the same lines, Lin et al.[117] found that by promoting $PC_{61}BM$ aggregation into large domains within the ETL by using a block co-polymer (PS-b-PEO) with a large disparity in polarity, they could improve the electron transport ability. Although $PC_{61}BM$ aggregation did not lead to crystallinity

in the ETL, by controlling the amount of block co-polymer, the authors were able to tune the phase separation in the ETL and improve the PCE by 4% relative to the control devices. Beyond the morphological considerations of the fullerene/perovskite layers, fullerene functionalization can also have a remarkable effect on device performance.

4.1 Fullerenes as compact layers

Fullerenes and their derivatives are the most used n-type ETMs in inverted PSCs due to their efficient electron transporting and solution processable properties, low temperature fabrication, suitable energy level alignment with that of the perovskites, and acceptable electron mobilities.[118,119] Besides $PC_{61/71}BM$[68,78,80,120] (2 and 4, Fig. 3) or $PC_{61}BM$ as additives,[1,84] other fullerene derivatives have also been used as efficient ETMs in PSCs (Fig. 3).[62–64,66,70,72,74,76,85,90,108,121–124] To date, it is still not fully understood why fullerenes and their derivatives act so well as ETMs in PSCs. In this section, we review the most import findings based on $PC_{61/71}BM$ and different fullerene derivatives that have been synthesized to study the role of the functional group.

Recently, we reported the synthesis and photovoltaic applications of $DMEC_{60}$ and $DMEC_{70}$, compounds 6 and 7, respectively (Fig. 3). We found that inverted PSCs based on 6 or 7 as ETMs exhibited both higher PCE and higher device-stability compared to devices based on the $PC_{61/71}BM$. These results were attributed to the ability of the $DMEC_{60/70}$ to extract electrons more efficiently, likely due to specific interactions between the pyrrolidine groups (carbonyls and amino groups) and the perovskite crystals at the interfaces, as determined by infrared (IR) spectroscopy.[62,125] Due to the suitable energy levels and good electron mobility of $PC_{61}BM$-dimers, they have been used as efficient electron acceptors in organic solar cells OSCs.[126,127] Taking this into account, we have reported,[63] for the first time, the use of a $PC_{61}BM$-dimer, (D-C_{60}) compound 8 (Fig. 3), as the ETM in inverted PSCs. The results showed improved PCE and device stability as compared to devices based on $PC_{61}BM$. This improved performance was attributed to effective perovskite film surface passivation as well as improved electron extraction and transport efficiency, as determined by photoluminescence (PL) techniques and electrochemical impedance (EIS). Han et al.[123] reported the use of a blend composed of $PC_{61}BM$: $PC_{61}BM$-dimer (d-$PC_{61}BM$, compound 9) with a 4:1 ratio, respectively, to control the morphology and the electron transporting ability of the ETL. Higher PCEs were obtained from the mix-based devices compared to those for the pure $PC_{61}BM$-based devices.

Xing et al.[64] synthesized several C_{60} and C_{70} fullerene derivatives functionalized with oligoether chains, compounds 10–14 (Fig. 3), and used as ETMs to study trap passivation mechanisms in inverted PSCs. These new materials are good candidates for replacing $PC_{61/71}BM$ layers. The results show that the length of the oligoether chains affect the energy levels, charge carrier mobilities, surface energy and dipole layer features at the interfaces. In many cases, improved device performance has been attributed to the fullerene design for both electronic and
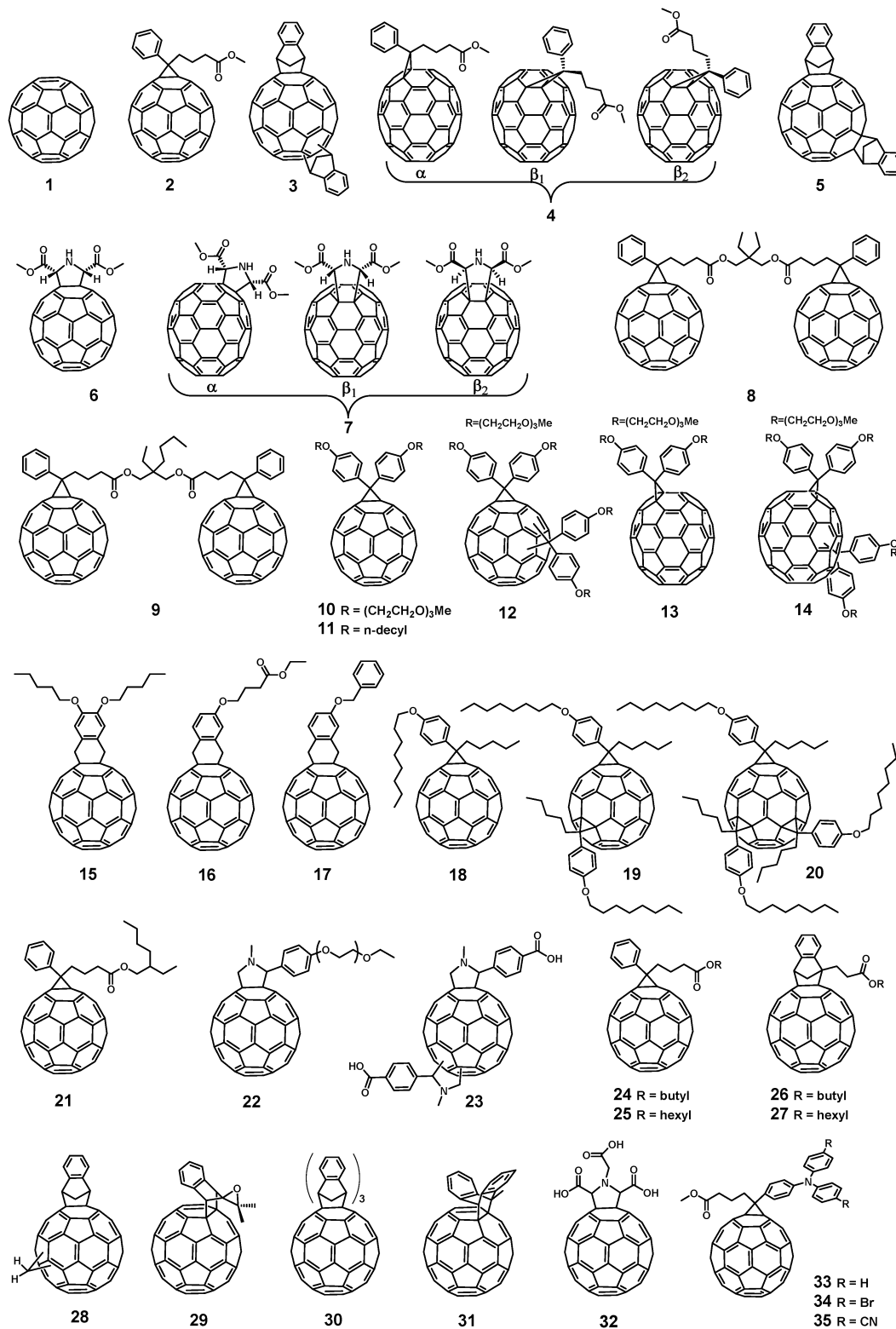
Fig. 3 Structures of the fullerene derivatives used as ETMs in PSCs.

morphological reasons. Meng *et al.*[70] reported that by using C5-NCMA, compound **15** (Fig. 3), as the ETM in inverted PSCs, both higher efficiencies and longer device-stabilities, as compared to those of PC$_{61}$BM-based devices, were achieved. The high PCE

values were attributed to the high electron mobility, efficient charge extraction and improved electron transport ability of **15** (Fig. 3). The Improved stabilities of devices based on **15** was mainly due to its hydrophobicity. Dai *et al.*[124] investigated the effects of

EDNC and BDNC compounds 16 add 17, respectively, as the ETM in PSCs. 16-based devices exhibited higher PCEs than 17-based devices and the results were attributed to the smoother surface morphology of the films with 17. The electron mobility of $PC_{61}BM$ is approximately one order of magnitude higher than that of 16 and 17, which yielded higher J_{sc} and FF when compared to 16-based devices, thus demonstrating the importance of electron mobility, as well as surface morphology, on fullerene-based PSCs. Similarly, Zhang et al.[128] reported that due to the low electron mobility of compounds 18–20 (Fig. 3), charge carriers can accumulate at the perovskite/fullerene interface, leading to an electric field that gives rise to the notorious hysteretic behavior. By replacing the methyl group of the $PC_{61}BM$ for the 2-ethylhexyl group of $PC_{61}BEH$ (compound 21, Fig. 3), it was found that $PC_{61}BEH$ exhibits increased solubility without affecting the electron mobility nor the HOMO/LUMO energy levels, which resulted in improved overall device performance.[103]

One common issue in PSCs is the light-soaking-effect (performance variation under illumination). To address this phenomenon Shao et al.[72] studied how fullerene derivatives with different dielectric constants (compound 22, dielectric constant 5.9) (Fig. 3) can eliminate the light-soaking-effect. As shown in Fig. 4, the photo-generated electrons are injected into the ETL, where they are either collected by the cathode or captured by surface traps, resulting in non-radiative recombination (r_c). The latter can be determined using eqn (1):

$$r_c = \frac{q^2}{4\pi\varepsilon_0\varepsilon_r kT} \qquad (1)$$

where q, T, ε_0 and ε_r are the elementary charge, temperature, vacuum permittivity and the dielectric constant of the ETM, respectively. The electrons that are within r_c distance have higher probability to be trapped. From eqn (1), the higher the ε_r the smaller the r_c.

Erten-Ela et al.[66] reported the synthesis and application of the benzoic acid fullerene bis-adduct 23 (Fig. 3). Although the PCE for devices based on this compound are not better than for $PC_{61}BM$-based devices, higher J_{sc} values were obtained when 22 was used as the ETM in PSCs. The effect of the $PC_{61}BM$- and indene-alkyl chain (compounds 24–27) (Fig. 3) as the ETM in PSCs was studied by Gil-Escrig et al.[106] The derivatives with longer alkyl chain (compounds 25 and 27) led to improved layers with fewer defects than those obtained with $PC_{61}BM$. As expected, indene-based devices exhibited higher V_{oc} than those

of $PC_{61}BM$-like based devices, which is attributed to the energetically high-lying LUMO levels. An indene bis-adduct derivative, compound 28 (Fig. 3) was used as the ETM in PSCs by Xue et al.[108] Compared to $PC_{61}BM$-28-based devices exhibited higher V_{oc} and higher overall performance, which was mainly attributed to the higher energy LUMO value of 28. Chang et al.[74] reported that IBF-Ep compound 29 (Fig. 3) can be used as the ETM in both regular and inverted PSCs, though better results were obtained when 29 (Fig. 3) was used in inverted structures. Wolff et al.[90] investigated how fullerenes 1, 2 and 30 (Fig. 3) affect the V_{oc} values in inverted PSCs, when a thin layer of an insulator polymer is in between the perovskite and the ETM interface. The results showed that the insulator interlayer reduces the recombination process and improves the electron extraction from the perovskite layer, which is more effective than raising the LUMO level of the ETMs (compound 30) (Fig. 3). The influence of additives in the fullerene layer has also been studied. It was reported that the addition of polystyrene (PS) into the $PC_{61}BM$ solution, leads to the formation of a smooth and uniform ETL, resulting in an improved overall device performance.[84] When cetyltrimethyl-ammonium bromide (CTAB) was added into the $PC_{61}BM$ layer, good film coverage was observed, and both improved PCE values and device stabilities were obtained. This approach was also used to fabricate large-area devices (1.2 cm^2) to prove the applicability of the method.[129] Pyridine,[130] graphdiyne,[131] hexamethonium bromide,[129] cetyltrimethylammonium bromide,[129] 1,3-dimethyl-2-phenyl-2,3-dihydro-1H-benzoimidazole (DMBI),[132] reduced graphene oxide[133] and oleamide[134] have also been used as an additive to improve electron mobility, decrease series resistance and smooth the surface of the $PC_{61}BM$ layer. Umeyama et al.[76] reported for the first time the use of C_{60} thin films as the ETM in regular PSCs, after thermal retro-Diels–Alder reaction on as-prepared glass/FTO/C_{60}-9-methylanthracene (31) (Fig. 3). Higher fill factor (FF) values and lower charge-transfer resistance from ETM/perovskite interfaces compared with the commonly used TiO$_2$-based devices were obtained. Recently, Wang et al.[135] reported that compound 32 (Fig. 3) can be covalently anchored onto the ITO surface, and used as the ETM in regular PSCs as represented in Fig. 5. The main photovoltaic characteristics of PSCs-based on compounds 1–35 are summarized in Table 1.

Compound 32 (Fig. 3) shows good electron mobility and HOMO/LUMO values that match those of the perovskite. Devices based on this compound as the ETM showed negligible
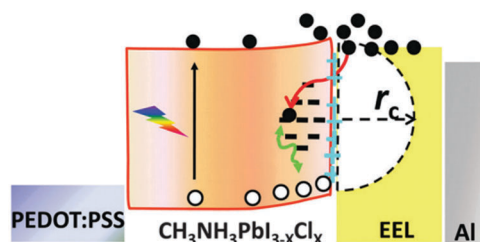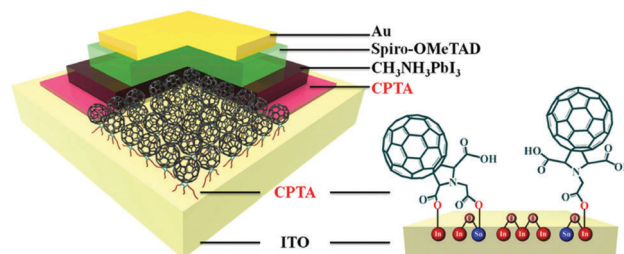

Fig. 4 Proposed mechanism for the light-soaking-effect, reproduced with permission from ref. 72. Copyright 2016, Royal Society of Chemistry.

Fig. 5 Schematic device structure of planar regular perovskite solar cells using fullerene 32 as the ETL. Reproduced with permission.[135] Copyright 2017, John Wiley and Sons.

hysteretic behavior and a remarkable device stability, achieving maximum PCE values of 18.39% and 17.04% for rigid and flexible devices, respectively. Li et al.[136] reported an approach to modulate the fullerene/perovskite interface, which resulted in improved device performance when fullerenes 33–35 (Fig. 3) were used as the ETMs. Fullerenes with excited transfer states (33 and 34) showed almost no fullerene photoluminescence, enhanced molecular polarization and higher electron transport capabilities compared to $PC_{61}BM$.

4.2 Fullerenes as interfacial modification layers

Although PSCs based on meso-porous TiO_2 are leading the race in terms of PCE values, PSCs based on planar structures are becoming more popular due to their simple architecture and lower temperature processability. Lower temperature processed TiO_2 can also serve as an ETM in regular PSCs due to its good conduction band match with those of the hybrid perovskites and its deep valence band, which can block the holes.[10] However, the low electron mobility of the compact TiO_2 layer leads to charge accumulation at the interface, resulting in charge-recombination.[137]

Snaith and other groups have demonstrated that coating the TiO_2 with a thin layer of $PC_{61}BM$ or by modifying the TiO_2 surface with a self-assembled monolayer (SAM) of fullerene derivatives (compounds 36–45, Fig. 6), reduces the non-radiative recombination channels at the interface thus reducing the hysteresis and enhancing device performance.[79,85–87,91,95,98,102,105,138,139] The SAMs not only provide a valuable reference to explore the fundamentals of hysteresis, but also introduce a technical and viable concept to large-area processing of hysteresis-free solar cells. In a similar approach, water soluble fullerene derivatives (compounds 42 and 43, Fig. 6) were deposited between the $PC_{61}BM$/perovskite layer in regular PSCs.[88,96] The second fullerene layer not only improves the wettability of the perovskite film on the ETL but also increases the electron transport ability across the interface between the perovskite and TiO_2 layers. To avoid damage of the C_{60} layer deposited on top of the ITO, the latter was coated with polyethylenimine ethosylated (PEIE) to keep the integrity of the C_{60} film.[67] Results showed that the ETL is an effective template to grow high-quality $MAPbI_3$-based perovskite layers.

When $PC_{61}BA$, compound 44 (Fig. 6), was used as an interfacial modification monolayer between the perovskite/c-TiO_2 interface, a PCE improvement was observed, from 7.46% without the fullerene derivative to 17.76% for 44-based devices under reverse scan.[105]

Table 1 Summary of the PSCs performance based on compounds 1–35

Compound	Perovskite	μ (cm^2 V^{-1} s^{-1})	LUMO (eV)	J_{sc} (mA cm^{-2})	V_{oc} (V)	FF (%)	PCE (%)	Ref.
1	$MAPbI_3$	10^{-3}	−4.01	21.7	1.03	0.74	16.49	90
2	$FA_{0.85}MA_{0.15}Pb(I_{0.85}Br_{0.15})_3$	1.3×10^{-3}	−3.91	23.7	1.03	0.79	19.2	26
3	$(FA_{0.83}MA_{0.17})_{0.95}Cs_{0.05}Pb(I_{0.6}Br_{0.4})_3$	4.5×10^{-5}	−3.7	18.0	1.11	0.73	14.6	61
4	$MAPbI_3$	1.0×10^{-3}	−3.91	23.51	1.03	0.83	20.1	24
4α	$MAPbI_3$	1.5×10^{-4}	−3.87	19.70	0.87	0.55	9.37	120
4β$_1$	$MAPbI_3$	1.7×10^{-4}	−3.87	1.68	0.80	0.23	0.38	120
4β$_2$	$MAPbI_3$	2.4×10^{-4}	−3.87	11.57	0.79	0.41	3.70	120
5	$(FA_{0.83}MA_{0.17})_{0.95}Cs_{0.05}Pb(I_{0.6}Br_{0.4})_3$	3.1×10^{-4}	−3.7	19.7	1.20	0.78	18.3	61
6	$MAPbI_3$	7.21×10^{-4}	−3.89	21.73	0.92	0.76	15.2	62
7	$MAPbI_3$	9.07×10^{-4}	−3.90	22.44	0.95	0.77	16.4	62
7α	$MAPbI_3$	9.98×10^{-4}	−4.24	22.88	1.02	0.80	18.6	125
8	$MAPbI_3$	9.83×10^{-4}	−3.88	21.89	0.96	0.79	16.6	63
9	$MAPbI_{3-x}Cl_x$	—	—	17.01	0.96	0.74	11.7	123
10	$MAPbI_{3-x}Cl_x$	5.0×10^{-4}	−3.88	21.4	0.96	0.76	15.5	64
11	$MAPbI_{3-x}Cl_x$	1.1×10^{-4}	−3.81	19.9	0.90	0.60	10.8	64
12	$MAPbI_{3-x}Cl_x$	1.8×10^{-5}	−3.99	20.7	0.93	0.71	13.8	64
13	$MAPbI_{3-x}Cl_x$	3.3×10^{-4}	−3.86	21.9	0.97	0.75	16.0	64
14	$MAPbI_{3-x}Cl_x$	1.7×10^{-5}	−4.01	21.0	0.94	0.71	14.0	64
15	$MAPbI_3$	1.59×10^{-3}	−3.87	20.68	1.08	0.79	17.6	70
16	$MAPbI_3$	8.5×10^{-5}	−3.86	19.85	0.95	0.67	12.64	124
17	$MAPbI_3$	7.5×10^{-5}	−3.86	16.17	0.93	0.49	7.36	124
18	$MAPbI_3$	8.8×10^{-4}	−3.74	10.30	1.04	0.44	3.72	128
19	$MAPbI_3$	2.6×10^{-4}	−3.65	2.10	1.03	0.65	1.39	128
20	$MAPbI_3$	2.7×10^{-7}	−3.56	1.71	1.03	0.74	0.74	128
21	$MAPbI_3$	4.8×10^{-4}	−3.89	22.5	0.95	0.78	16.26	103
22	$MAPbI_{3-x}Cl_x$	—	−3.91	20.63	0.94	0.81	15.71	72
23	$MAPbI_3$	—	−3.86	16.21	0.83	0.70	9.21	66
24	$MAPbI_3$	—	−3.91	16.02	1.09	0.76	13.27	106
25	$MAPbI_3$	—	−3.91	15.92	1.10	0.79	13.75	106
26	$MAPbI_3$	—	−3.94	16.28	1.10	0.78	14.02	106
27	$MAPbI_3$	—	−3.94	16.70	1.18	0.79	14.64	106
28	$MAPbI_3$	3.0×10^{-3}	−3.66	20.4	1.13	0.80	18.1	108
29	$MAPbI_{3-x}Cl_x$	—	−4.40	16.1	1.00	0.43	6.9	74
30	$MAPbI_3$	—	—	21.3	1.10	0.74	18.04	90
31	$MAPbI_3$	—	—	21.1	0.98	0.72	15.0	76
32	$MAPbI_3$	5.4×10^{-3}	−3.9	22.06	1.10	0.76	18.39	135
33	$MAPbI_{3-x}Cl_x$	7.90×10^{-4}	—	18.25	0.90	0.71	11.38	136
34	$MAPbI_{3-x}Cl_x$	3.32×10^{-4}	—	17.61	0.91	0.72	10.58	136
35	$MAPbI_{3-x}Cl_x$	7.21×10^{-4}	—	14.13	0.92	0.51	6.41	136
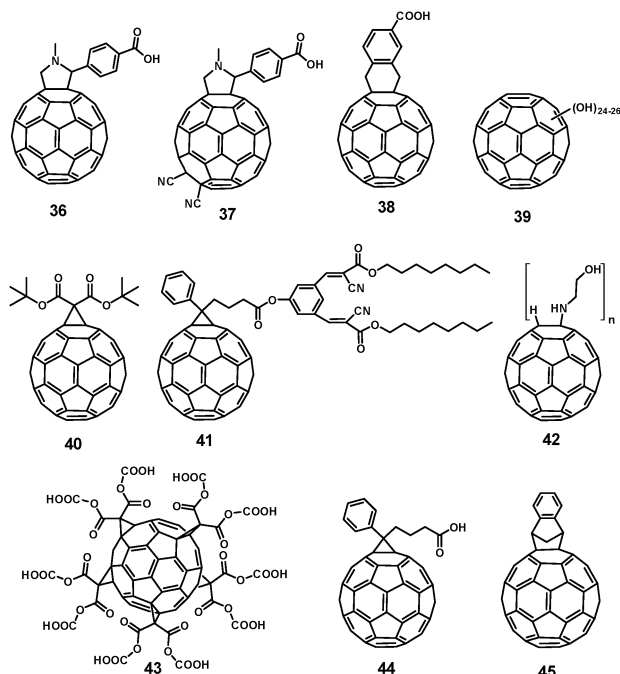
Fig. 6 Structure of the fullerene derivatives used as interlayers in inverted PSCs.
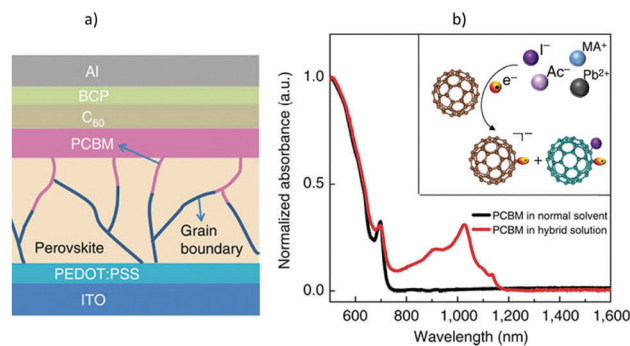

Fig. 7 (a) Passivation process mediated by $PC_{61}BM$ permeation. Adapted with permission from ref. 17. Copyright 2014, Nature Publishing Group. (b) UV-Vis absorption spectrum of the hybrid solution showing the interaction between $PC_{61}BM$ and perovskite ions. Adapted with permission from ref. 110. Copyright 2015, Nature Publishing Group.

When compound **45** was used as a monolayer it led to effective passivation of the trap sites on the c-TiO₂, reduced the hole recombination at the cTiO₂/perovskite interface, facilitated the electron extraction and improved the morphology of the perovskite film, which led to a better overall device performance.[105] Kegelmann *et al.*[107] reported the influence of **1**, **2** and **45** as interfacial modifiers on PSCs. It was found that only the ETL double layer (TiO₂/$PC_{61}BM$) led to higher efficiency with negligible photocurrent hysteresis, which can be attributed to reduction of shunt paths through the fullerene to the ITO layer, decreased transport losses and improved hole blocking by the wide band gap metal oxide.

4.3 Fullerenes as additives

Huang and coworkers[73,140] demonstrated that the spun $PC_{61}BM$ layer can permeate into the perovskite layer throughout the grain boundaries during the annealing process below 100 °C (Fig. 7a). Xu *et al.*[110] showed the formation of a $PC_{61}BM$ radical by UV-Vis spectroscopy. These results suggest that $PC_{61}BM$ is passivating the iodide trap sites on the surface grains. As shown in Fig. 7b, iodide reacts with $PC_{61}BM$ or C_{60} to form a bond by direct electron transfer to the fullerene. Different approaches have been developed to modify the morphology of perovskite solar films, aimed at improving stability and large-scale production capability. The main photovoltaic characteristics of PSCs based on compounds **36–56** are summarized in Table 2.

The use of fullerenes as additives within the perovskite solution,[52,69,92,111,112,141–144] in chlorobenzene as antisolvent[43,113] or by immersion of the as-prepared perovskite thin films into a fullerene solution,[65] has shown remarkable FFs up to 86.7%, negligible hysteretic behavior, improved long-term-device stability,

and last but not least, high PCE values for large-area-based devices. Fullerene derivatives **46–56** used as additives are shown in Fig. 8.

4.4 Fullerenes as cathode buffer layers, cross-linkable and double layers

The role of a cathode buffer layer in PSCs is to improve the metal electrode efficiency in collecting charge carriers. As discussed above fullerenes are excellent ETMs. However, a barrier exists at the contact interface between the Fermi level of different metal electrodes such as Al, Ag or Au and the LUMO of the fullerenes, which leads to poor electron injection and extraction. To minimize this barrier a quasi-ohmic contact at the fullerene/metal interface is needed.[145–150]

Jen's and Huang's groups, among others, have reported the use of different double fullerene layers to improve device performance in PSCs (compounds **57–60**, Fig. 9).[16,73,80,81,89,101,140,151–153] Cross linkable fullerene derivatives (**36**, Fig. 6 and **61–63**, Fig. 9) that enhance water and moisture stability have been reported,[71,75,93] as well as the use of fullerene salts (**58**, **64** and **65**, Fig. 9),[77,80,97] and polymers (**66**, Fig. 9)[94,99,154] to reduce the work function of the metal electrodes and prevent degradation caused by humidity.

Compounds **57** and **67** (Fig. 9) were used as interlayers to reduce the interface barrier and also to enhance the stability of PSC devices.[82,100,101] Enhanced photovoltaic performance and device stability were obtained using a **58**/**68** blend mixture[155] or by the incorporation of $MPMIC_{60}$, compound **69** (Fig. 9).[156] The main photovoltaic characteristics of PSCs-based on compounds **57–69** are summarized in Table 3.

5. Calculations of the perovskite/fullerene interface

Density functional theory (DFT) calculations and molecular dynamic (MD) simulations have been used to study the interfacial energy alignment and charge transfer properties at the perovskite/organic interface.[110,157–159] Yin *et al.*[157] reported an experimental and theoretical study of the energy level alignment and charge transfer properties at the perovskite/$PC_{61}BM$

Table 2 Summary of the PSCs performance based on compounds **36–56**

Compound	Perovskite	μ (cm² V⁻¹ s⁻¹)	LUMO (eV)	J_{sc} (mA cm⁻²)	V_{oc} (V)	FF (%)	PCE (%)	Ref.
36	MAPbI$_{3-x}$Cl$_x$	—	−3.95	22.1	1.04	0.75	17.3	85
37	MAPbI$_{3-x}$Cl$_x$	—	−4.20	19.4	0.79	0.76	10.8	95
38	MAPbI$_{3-x}$Cl$_x$	—	−4.00	19.8	0.85	0.71	11.7	95
39	MAPbI$_{3-x}$Cl$_x$	—	−4.27	21.28	0.96	0.72	14.7	91
40	MAPbI$_3$	—	−4.2	20.6	1.17	0.71	17.09	98
41	MAPbI$_3$	4.8×10^{-3}	−4.01	20.68	1.06	0.79	17.35	79
42	MAPbI$_3$	—	−3.72	23.76	1.06	0.69	18.49	96
43	MAPbI$_3$	—	−4.1	27.4	0.95	0.56	14.6	88
44	MAPbI$_3$	—	−4.2	16.97	1.09	0.71	13.15	105
45	MAPbI$_3$	—	−3.85	20.2	1.06	0.46	12.8	107
46	MAPbI$_3$	—	—	15.4	1.04	0.73	11.7	141
47	MAPbI$_3$	—	−4.06	16.7	1.03	0.69	11.8	112
48	MAPbI$_3$	—	−4.08	16.1	1.02	69.4	11.7	112
49	MAPbI$_3$	—	−4.05	16.1	1.06	73.8	12.7	112
50^a	MAPbI$_3$	—	−4.08	—	—	—	—	112
51	MAPbI$_3$	—	−3.97	16.1	1.04	69.2	11.6	112
52	MAPbI$_3$	1.8×10^{-3}	—	21.29	1.10	0.79	18.53	69
53	MAPbI$_3$	—	−3.72	20.7	1.09	0.73	16.41	114
54	MAPbI$_3$	—	−3.64	17.8	1.06	0.76	15.07	114
55	MAPbI$_3$	—	−3.69	18.5	1.07	0.78	16.37	114
56	(FAI)$_{0.81}$(PbI)$_{20.85}$(MABr)$_{0.15}$(PbBr$_2$)$_{0.15}$	62.30^b	—	23.95	1.13	0.74	20.8	43

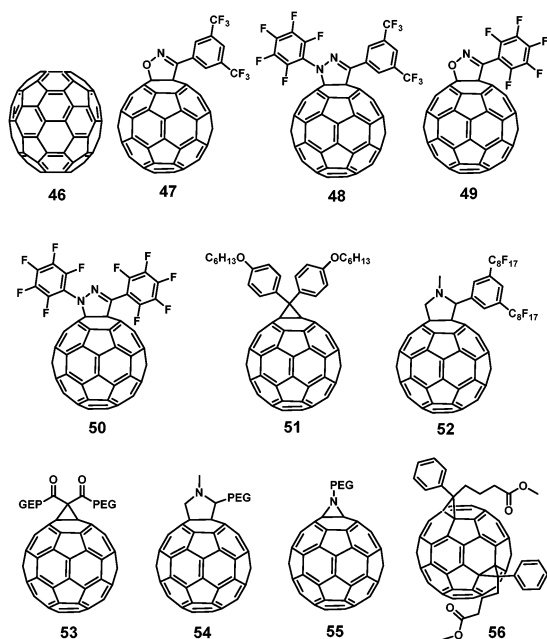^{a} Not testes because its low solubility. ^{b} Obtained from the hall effect measurement.

Fig. 8 Structure of fullerene derivatives used as perovskite-additives.

interface. Theoretical results agree well with experimental ultraviolet photoelectron spectroscopy (UPS) measurements, showing that the polar CH$_3$NH$_3$PbI$_3$ (100) surface facilitates electron transfer to PC$_{61}$BM largely delocalized surface states and orbital coupling (Fig. 10a). Xu et al.[110] confirmed the strong PC$_{61}$BM–iodide interaction using DFT calculations. It was found that the wavefunction of the ground state was hybridized between the perovskite/PC$_{61}$BM interface (Fig. 10b). Quarti et al.[158] reported that the electronic energy alignment and charge transfer from the perovskite to C$_{60}$ depend on the perovskite surface termination. The conduction band edge (CBE) of the

MAI-terminated perovskite lies above the LUMO of the C$_{60}$, allowing a spontaneous charge transfer of the photogenerated electron into the C$_{60}$, while the CBE of the PbI-terminated perovskite lies below the LUMO of the C$_{60}$, avoiding electron injection (Fig. 10c). Taufique et al.[159] performed MD simulations of PC$_{61}$BM solvated in chlorobenzene near the (100) and (110) perovskite surface. PC$_{61}$BM showed orientational preferences in which the carbonyl oxygen atoms interact with the Pb and H atoms of (100) and (110) faces of perovskite (Fig. 10d).

6. Device Stability

6.1 Humidity, oxygen and light exposure

One of the external factors that affects the stability of PSCs is humidity. Exposure of the device to the atmosphere can completely degrade it in just a few days, even when stored in the dark. Yang et al.[160] reported that the degradation rate is affected not only by the relative humidity (RH) but also by the nature of the HTM. Christians et al.[161] reported that the degradation of the perovskite starts with the formation of a hydrate at the perovskite surface, and then propagates through the entire perovskite layer[161] as represented in eqn (2).

Additionally, Leguy et al.[163] found that the degradation process occurs in two steps and is water exposure dependent (Fig. 11). When heat is combined with moisture, unlike the previous processes, it leads to a complete irreversible degradation of the perovskite layer, yielding PbI$_2$ and the degraded organic counterpart.[164]

$$CH_3NH_3PbI_3 + H_2O \rightarrow (CH_3NH_3)_4PbI_6 \cdot 2H_2O \qquad (2)$$
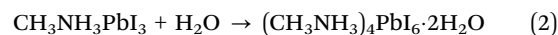
Several studies have tried to overcome these problems and increase device stability under atmospheric conditions. Noh et al.[11] reported that the use of Br⁻ as the halide in the
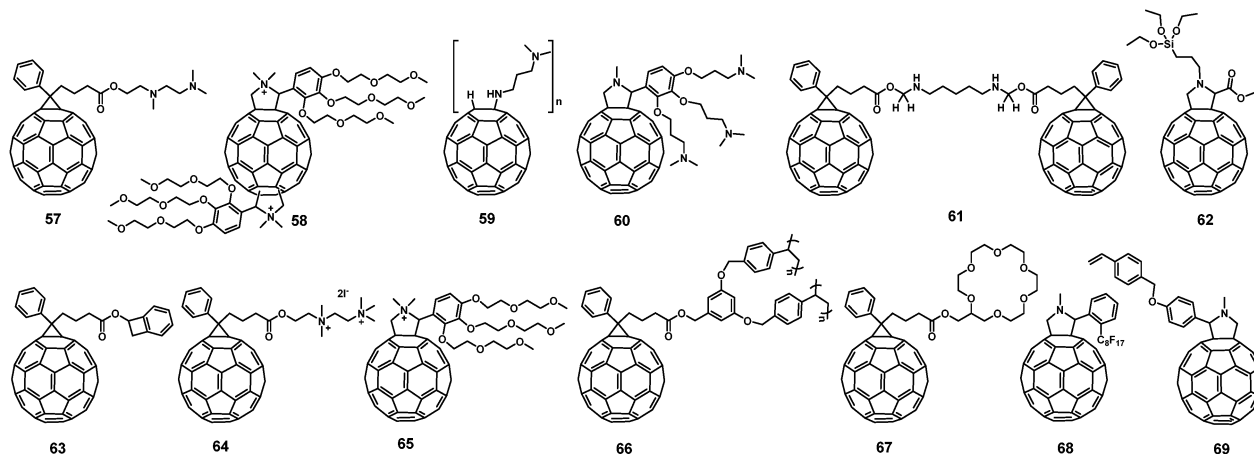
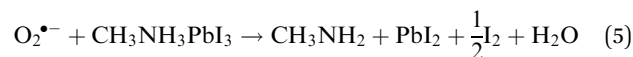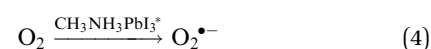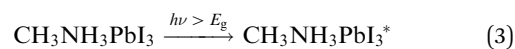**Fig. 9** Structure of fullerene derivatives used as cathode buffer layers and double layers.

Table 3 Summary of the PSCs performance based on compounds **57–69**

Compound	Perovskite	μ (cm^2 V^{-1} s^{-1})	LUMO (eV)	J_{sc} (mA cm^{-2})	V_{oc} (V)	FF (%)	PCE (%)	Ref.
57	MAPbI$_3$	—	−4.1	21.70	1.08	0.77	18.1	153
58	MAPbI$_3$	—	—	21.07	0.92	0.80	15.44	80
59	MAPbI$_{3-x}$Cl$_x$	—	—	17.9	0.97	0.77	13.4	81
60	MAPbI$_3$	—	−3.9	20.50	1.03	0.74	15.50	151
61	MAPbI$_3$	—	—	20.3	19.5	77.9	17.1	71
62	MAPbI$_{3-x}$Cl$_x$	3.8×10^{-4}	—	23.0	1.07	0.73	17.9	75
63	MAPbI$_{3-x}$Cl$_x$	5.9×10^{-3}	—	22.4	1.11	0.73	17.9	75
64	MAPbI$_{3-x}$Cl$_x$	—	−3.68	21.28	0.91	0.81	15.71	77
65	MAPbBr$_3$	—	−3.9	5.50	1.33	0.74	5.44	97
66	MAPbI$_3$	—	—	22.81	0.98	0.77	17.21	99
67	MAPbI$_{3-x}$Cl$_x$	—	—	22.08	0.98	0.70	15.08	82
68	MAPbI$_{3-x}$Cl$_x$	—	—	21.2	0.97	0.75	15.5	155
69	MAPbI$_3$	—	−4.1	20.2	1.08	0.64	13.8	156

perovskite film strengthens the hydrogen bonding between CH$_3$NH$_3^+$ and [PbI$_6$]$^{4-}$ and avoids the formation of hydrates. Similar work, done by Jiang et al.[165,166] introduced SCN$^-$ instead of Br$^-$ to increase device stabilities. With this modification, no degradation of the device was observed under conditions up to 70% RH. Another strategy to improve device stability relies on the use of fullerene derivatives, which have high hydrophobicity and form compact self-assembled layers, thus avoiding water insertion and subsequent device degradation.[70,74] Oxygen also influences device degradation, it oxidizes the organic material in the cell, but unlike moisture degradation, oxygen can have a greater effect when exposed to light.[167,168] This phenomenon has been observed to occur by a well-studied photo-oxidation process.[169] This process is dominated by electron transfer and oxidation rates. Oxidation of the semiconductor is prevalent except for the case when the electron transfer rate is dominant.[164,169] The mechanism by which the perovskite degrades in the presence of oxygen and light is represented in eqn (3)–(5).[162,170] When light strikes the perovskite, it forms a non-equilibrated population of electrons and holes (eqn (3)).

Then electrons from the conduction band form a superoxide anion with the adsorbed oxygen from the atmosphere (eqn (4)). Finally, methylammonium cation is deprotonated and the iodide anion is oxidized by the superoxide anion (eqn (5)).[162,170]

Aristidou et al.[13] reported that the O$_2^{\bullet-}$ formation rate can be decreased by using interlayers that are able to extract electrons from the perovskite film before they can react with the oxygen to form the superoxide.[170,171] To date, the best way to delay the degradation process caused by moisture and oxygen is by device encapsulation.[9,162,164]

$$CH_3NH_3PbI_3 \xrightarrow{h\nu > E_g} CH_3NH_3PbI_3^* \qquad (3)$$

$$O_2 \xrightarrow{CH_3NH_3PbI_3^*} O_2^{\bullet-} \qquad (4)$$

$$O_2^{\bullet-} + CH_3NH_3PbI_3 \rightarrow CH_3NH_2 + PbI_2 + \tfrac{1}{2}I_2 + H_2O \qquad (5)$$

6.2 Thermal instability

To understand the thermal decomposition, different parameters have been considered.[172–174] Yang et al.[175] reported that after heating the perovskite layer decomposes to generate PbI$_2$ in one step. It has also been reported that decomposition depends on the heating time, applied temperature and the nature of the ETL, as shown in Fig. 12a and b.[175–177] Device decomposition was characterized by XRD studies.[17–20] The mechanism represented in eqn (6) and (7) was proposed to
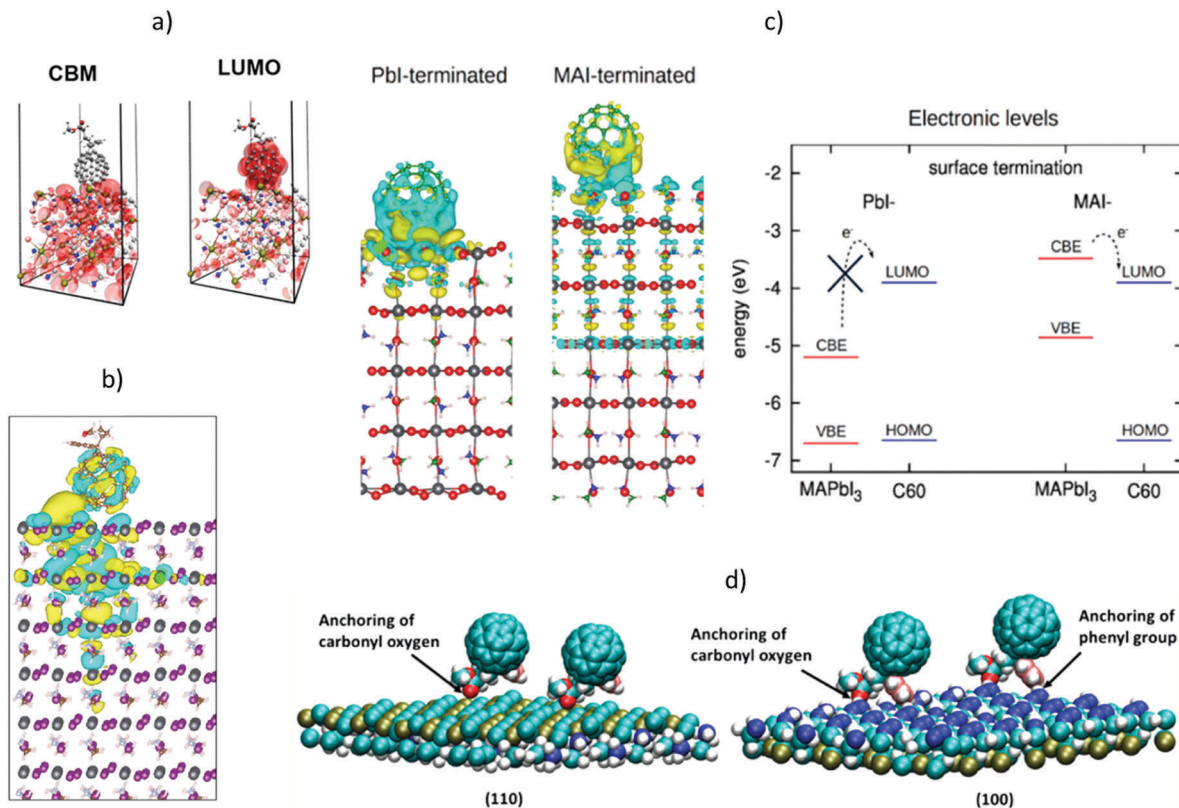
Fig. 10 Calculations at the perovskite/fullerene interface. (a) Three-dimensional representation of CBM and LUMO levels at the $PC_{61}BM/CH_3NH_3PbI_3$ (100) surface, with isovalue of 5×10^{-4} e $Å^{-3}$. Adapted with permission from ref. 157. Copyright 2015 American Chemical Society. (b) Hybridization between $PC_{61}BM$ and defective surface. Adapted with permission from ref. 110. Copyright 2015, Nature Publishing Group. (c) C_{60} interacting with the PbI-terminated perovskite (001) surface and MAI-terminated perovskite (001) surface, and the CBE of the MAI-terminated perovskite allowing charge transfer into C_{60}, while the CBE of the PbI-terminated perovskite avoids electron injection. Adapted with permission from ref. 158. Copyright 2017 American Chemical Society. (d) MD simulations of $PC_{61}BM$ interacting with the Pb and H atoms of (100) and (110) faces of perovskite. Adapted with permission from ref. 159. Copyright 2015 American Chemical Society.
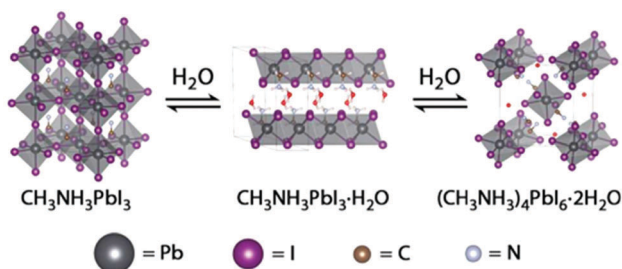

Fig. 11 Hydration process for the perovskite film. Reproduced with permission.[162] Copyright 2017, American Chemical Society.
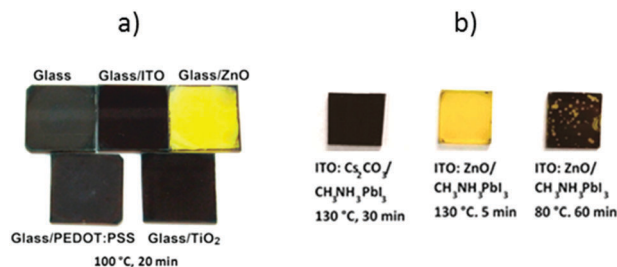

Fig. 12 Decomposition of the perovskite layers using different ETLs, under varied times and temperatures. (a) Adapted from ref. 175 with permission. Copyright 2015, American Chemical Society. (b) Adapted from ref. 177 with permission. Copyright 2014, American Chemical Society.

explain the degradation process due to temperature.[162,178] It was reported that degradation can also occur at 100 °C and without exposure to moisture.[179,180] Recent reports showed that decomposition can occur in the absence of humidity.[170,171,181] Decomposition is accelerated in the presence of light and oxygen as shown in eqn (2)–(4).[162,170]

$$OH^- + CH_3NH_3I \rightarrow CH_3NH_3OH + I^- \qquad (6)$$

$$CH_3NH_3OH \xrightarrow{heat} CH_3NH_2 \uparrow + H_2O \uparrow \qquad (7)$$

6.3 Fullerenes and their role in device stability

As discussed before, device stability is a very important factor for PSCs. In this regard the use of fullerene derivatives to restrict water intrusion, and thus prevent degradation at the interfaces and to passivate the grain boundaries in the perovskite layer even at high temperature (85 °C), is a good strategy to extend the integrity of the PSCs-based devices. Zang et al.[43] reported that PSCs fabricated using α-bis-PCBM, compound **56** (Fig. 8),
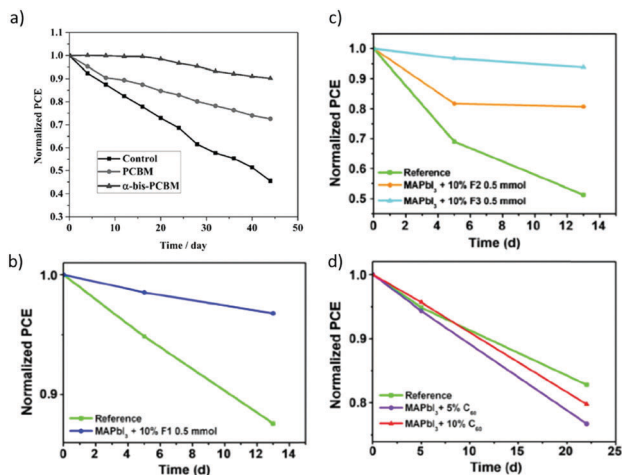
Fig. 13 Stability of fullerene-based PSCs. (a) Using compound **56**. Reproduced with permission.[43] Copyright 2017, John Wiley and Sons. (b) Using compound **53**, (c) using compound **54** and (d) using compound **55**. Reproduced with permission.[114] Copyright 2018, John Wiley and Sons.

as an additive exhibited a very substantial stability increase. As shown in Fig. 13a **56**-based PSCs kept 90.1% of their initial PCE after 44 days at 64 °C without encapsulation, compared to 72.6% and 45.4% for devices fabricated with $PC_{61}BM$ and without fullerene, respectively, under the same conditions. Collavini et al.[114] reported the use of fullerenes functionalized with polyethylenglycol (PEG) groups, compounds **53–55** (Fig. 8), as additives in PSCs. The fullerene–PEG derivates can interact with water by hydrogen bonding and thus inhibit the water intrusion into the perovskite layer. As shown in Fig. 13b and c, PSCs-based on **53–55** exhibited increased stability with respect to the reference device (without fullerene) at 97%, 81% and 94% of the initial PCE, respectively, after 13 days of ambient exposure. The enhanced stability was attributed to the fullerene's addend rather than the fullerene cage, as PSCs-based on C_{60} showed no improved stability compared with the control (Fig. 13d).

7. Considerations for the synthesis of new fullerene derivatives

There has been considerable progress in the use of fullerenes to improve the performance of PSCs. Many reported fullerenes perform better that the standard $PC_{61}BM$, yet there is no in-depth knowledge of the role of the fullerene or de addends in PSCs performance. Using recently reported works as a guide, here we list some important considerations for the synthesis of new fullerenes to be used in PSCs.

Compared to inorganic ETMs, fullerenes are an excellent alternative for the fabrication of PSCs due to their solubility in organic solvents, which allows device fabrication at a relative low temperature (below 100 °C). This allows the fabrication of flexible devices using these materials.[135]

We and other groups[103,106] have studied the effect of the fullerene addend on the performance of PSCs. It has been shown that fullerene solubility can be enhanced by attaching

longer alkyl chains, which improves film morphology, and increases both passivation and electron extraction ability. The challenge is to add a group that induces high fullerene solubility without interrupting other important properties such as electron mobility. Unfortunately, in many cases solubility is accompanied by lower electron mobilities.[128,182] It is well known that fullerenes $(10^{-3}-10^{-4}\ cm^2\ V^{-1}\ s^{-1})$ have 3–5 orders of magnitude lower electron mobility than perovskites (6–200 $cm^2\ V^{-1}\ s^{-1}$),[183] which affects the series resistance and FF. In this regard solubility and electron mobility need to be balanced when designing and synthesising new fullerene derivatives for PSCs.

Improvement of the V_{oc} values has been extensively studied[60,106,108] and typically, fullerenes with lower LUMO energy exhibit higher V_{oc} values. It has also been reported that the energy disorder in the ETL influences the V_{oc}. In this regard, a simple solvent annealing method to mitigate the energy disorder in the ETL that results in an improved V_{oc} was reported.[73] It was also found that the isomeric purity or a tuned isomeric mixture of fullerenes in the ETL has a considerable impact on the V_{oc}, and this effect can even reverse the expected results based solely on HOMO/LUMO energy level considerations.[120,125]

The long-term device stability has been improved using hydrophobic fullerenes, which minimize the penetration of water into the perovskite layer in inverted PSCs. We probed this concept by designing a $PC_{61}BM$ dimer that has similar energy levels and electron mobility but higher hydrophobicity than the monomer $PC_{61}BM$, resulting in an improved device-stability when the dimer was used as the ETM in inverted PSCs.[63]

Functionalization of fullerenes with groups that may have specific interactions with the perovskite material is another important consideration. We have reported that fullerenes functionalized with amino- and/or carbonyl groups can coordinate with the perovskite material and lead to enhanced device performance and long-term device stability.[62,125] It has also been reported that the crystal surface vacancies on the perovskites can be significantly passivated using organic Lewis bases such as thiophene and pyridine.[184] We hypothesize that fullerenes decorated with these moieties should yield interesting results.

8. Summary and perspectives

PCEs based on both regular and inverted PSC configurations have exceeded 20%, the latter using fullerene derivatives as the ETMs. Several fullerene derivatives with higher electron mobilities and hydrophobic properties, have been designed for improving device performance as well as device stability. By tuning the physical and chemical properties of fullerenes, enhanced charge extraction and transport capabilities were obtained.

By decreasing the structural disorder of fullerene derivatives layers, inverted PSCs with an improved V_{oc} comparable with that of TiO_2-based PSCs, can be fabricated. It is worth mentioning that PSCs based on fullerenes as the ETMs, perform better at eliminating the J–V hysteresis and can be fabricated at relatively low-temperature compared with those that use TiO_2 as the ETM.

PSCs are commercially promising because of their solution processable properties and high PCE values. Recent developments have shown that solution-based device fabrication can be achieved with high throughput, making PSC construction more industrially viable.[185] Large area devices, crucial to commercialization of PSCs, have also recently seen remarkable breakthroughs, with device sizes reaching 36 cm^2 with corresponding efficiencies of 12.07%.[186] Though still in its infancy as a technology, fullerene containing PSCs have shown to be a possible way forward toward commercialization of such devices as they are considerably more stable and thus more practical for real world applications.

Although a tremendous progress has been made toward increasing PCE values and device stability of PSCs, there are still many barriers to further overcome to compete with the inorganic-based solar cells that currently lead the market.

One of the main concerns for commercializing this technology is the long-term stability. PSCs have been exposed to drastic conditions such as long-time light-soaking conditions in the presence of air, and several research studies have been devoted to their stability under atmospheric conditions.[7,187–192] Cost-wise, less expensive organic materials are being used either as the ETMs or HTMs, which has motivated the research community to design new efficient materials.

Given the current trajectory of progress in this field of study, we foresee the development of new fullerene based PSC devices that will soon find commercial viability and rival older silicon based technology for market supremacy.

Conflicts of interest

There are no conflicts to declare.

Acknowledgements

References

1 B. K. Ghosh, C. N. J. Weoi, A. Islam and S. K. Ghosh, *Renewable Sustainable Energy Rev.*, 2018, **82**, 1990–2004.

2 M. K. Assadi, S. Bakhoda, R. Saidur and H. Hanaei, *Renewable Sustainable Energy Rev.*, 2017, **81**, 2812–2822.

3 W.-Q. Wu, D. Chen, R. A. Caruso and Y.-B. Cheng, *J. Mater. Chem. A*, 2017, **5**, 10092–10109.

4 NREL, Best Research-Cell Efficiencies, http://www.nrel.gov/pv/assets/images/efficiency_chart.jpg, accessed June 2017, June 2017.

5 M. Grätzel, *Acc. Chem. Res.*, 2017, **50**, 487–491.

6 X. Li, D. Bi, C. Yi, J.-D. Décoppet, J. Luo, S. M. Zakeeruddin, A. Hagfeldt and M. Grätzel, *Science*, 2016, **353**, 58–62.

7 S. S. Shin, E. J. Yeom, W. S. Yang, S. Hur, M. G. Kim, J. Im, J. Seo, J. H. Noh and S. I. Seok, *Science*, 2017, **356**, 167–171.

8 T. Ibn-Mohammed, S. C. L. Koh, I. M. Reaney, A. Acquaye, G. Schileo, K. B. Mustapha and R. Greenough, *Renewable Sustainable Energy Rev.*, 2017, **80**, 1321–1344.

9 T. Leijtens, K. Bush, R. Cheacharoen, R. Beal, A. Bowring and M. D. McGehee, *J. Mater. Chem. A*, 2017, **5**, 11483–11500.

10 J.-P. Correa-Baena, A. Abate, M. Saliba, W. Tress, T. Jesper Jacobsson, M. Grätzel and A. Hagfeldt, *Energy Environ. Sci.*, 2017, **10**, 710–727.

11 J. H. Noh, S. H. Im, J. H. Heo, T. N. Mandal and S. I. Seok, *Nano Lett.*, 2013, **13**, 1764–1769.

12 G. Xing, N. Mathews, S. Sun, S. S. Lim, Y. M. Lam, M. Gratzel, S. Mhaisalkar and T. C. Sum, *Science*, 2013, **342**, 344–347.

13 S. D. Stranks, G. E. Eperon, G. Grancini, C. Menelaou, M. J. P. Alcocer, T. Leijtens, L. M. Herz, A. Petrozza and H. J. Snaith, *Science*, 2013, **342**, 341–344.

14 J. T.-W. Wang, J. M. Ball, E. M. Barea, A. Abate, J. A. Alexander-Webber, J. Huang, M. Saliba, I. Mora-Sero, J. Bisquert, H. J. Snaith and R. J. Nicholas, *Nano Lett.*, 2014, **14**, 724–730.

15 T. Liu, K. Chen, Q. Hu, R. Zhu and Q. Gong, *Adv. Energy Mater.*, 2016, **6**, 1600457.

16 J. H. Kim, S. T. Williams, N. Cho, C.-C. Chueh and A. K. Y. Jen, *Adv. Energy Mater.*, 2014, **5**, 1401229.

17 Y. Deng, E. Peng, Y. Shao, Z. Xiao, Q. Dong and J. Huang, *Energy Environ. Sci.*, 2015, **8**, 1544–1550.

18 N. Marinova, S. Valero and J. L. Delgado, *Adv. Colloid Interface Sci.*, 2017, **488**, 373–389.

19 T. C. Sum and N. Mathews, *Energy Environ. Sci.*, 2014, **7**, 2518–2534.

20 G. Niu, X. Guo and L. Wang, *J. Mater. Chem. A*, 2015, **3**, 8970–8980.

21 L. K. Ono, M. R. Leyden, S. Wang and Y. Qi., *J. Mater. Chem. A*, 2016, **4**, 6693–6713.

22 Y. Zhou, O. S. Game, S. Pang and N. P. Padture, *J. Phys. Chem. Lett.*, 2015, **6**, 4827–4839.

23 J. Zhao, X. Zheng, Y. Deng, T. Li, Y. Shao, A. Gruverman, J. Shield and J. Huang, *Energy Environ. Sci.*, 2016, **9**, 3650–3656.

24 C.-H. Chiang, M. K. Nazeeruddin, M. Grätzel and C.-G. Wu, *Energy Environ. Sci.*, 2017, **10**, 808–817.

25 E. H. Anaraki, A. Kermanpur, L. Steier, K. Domanski, T. Matsui, W. Tress, M. Saliba, A. Abate, M. Gratzel, A. Hagfeldt and J.-P. Correa-Baena, *Energy Environ. Sci.*, 2016, **9**, 3128–3134.

26 X. Zheng, B. Chen, J. Dai, Y. Fang, Y. Bai, Y. Lin, H. Wei, Xiao C. Zeng and J. Huang., *Nat. Energy*, 2017, **2**, 17102.

27 E. L. Ratcliff, B. Zacher and N. R. Armstrong, *J. Phys. Chem. Lett.*, 2011, **2**, 1337–1350.

28 S. Yang, W. Fu, Z. Zhang, H. Chen and C.-Z. Li, *J. Mater. Chem. A*, 2017, **5**, 11462–11482.

29 H. Kim, K.-G. Lim and T.-W. Lee, *Energy Environ. Sci.*, 2016, **9**, 12–30.

30 J. Liu, G. Wang, K. Luo, X. He, Q. Ye, C. Liao and J. Mei, *ChemPhysChem*, 2017, **18**, 617–625.

31 W. S. Yang, B.-W. Park, E. H. Jung, N. J. Jeon, Y. C. Kim, D. U. Lee, S. S. Shin, J. Seo, E. K. Kim, J. H. Noh and S. I. Seok, *Science*, 2017, **356**, 1376–1379.

32 M. D. Birowosuto, D. Cortecchia, W. Drozdowski, K. Brylew, W. Lachmanski, A. Bruno and C. Soci, *Sci. Rep.*, 2016, **6**, 37254.

33 M. Liu, M. B. Johnston and H. J. Snaith, *Nature*, 2013, **501**, 395–398.

34 C. Momblona, L. Gil-Escrig, E. Bandiello, E. M. Hutter, M. Sessolo, K. Lederer, J. Blochwitz-Nimoth and H. J. Bolink, *Energy Environ. Sci.*, 2016, **9**, 3456–3463.

35 Q. Chen, H. Zhou, Z. Hong, S. Luo, H.-S. Duan, H.-H. Wang, Y. Liu, G. Li and Y. Yang, *J. Am. Chem. Soc.*, 2014, **136**, 622–625.

36 W. Zhang, M. Saliba, D. T. Moore, S. K. Pathak, M. T. Hörantner, T. Stergiopoulos, S. D. Stranks, G. E. Eperon, J. A. Alexander-Webber, A. Abate, A. Sadhanala, S. Yao, Y. Chen, R. H. Friend, L. A. Estroff, U. Wiesner and H. J. Snaith, *Nat. Commun.*, 2015, **6**, 6142.

37 Z. Song, S. C. Watthage, A. B. Phillips, B. L. Tompkins, R. J. Ellingson and M. J. Heben, *Chem. Mater.*, 2015, **27**, 4612–4619.

38 C. Roldan-Carmona, P. Gratia, I. Zimmermann, G. Grancini, P. Gao, M. Graetzel and M. K. Nazeeruddin, *Energy Environ. Sci.*, 2015, **8**, 3550–3556.

39 H. Zhou, Q. Chen, G. Li, S. Luo, T.-B. Song, H.-S. Duan, Z. Hong, J. You, Y. Liu and Y. Yang., *Science*, 2014, **345**, 542–546.

40 M. M. Lee, J. Teuscher, T. Miyasaka, T. N. Murakami and H. J. Snaith, *Science*, 2012, **338**, 643–647.

41 K. T. Cho, S. Paek, G. Grancini, C. Roldan-Carmona, P. Gao, Y. Lee and M. K. Nazeeruddin, *Energy Environ. Sci.*, 2017, **10**, 621–627.

42 N. Ahn, D.-Y. Son, I.-H. Jang, S. M. Kang, M. Choi and N.-G. Park, *J. Am. Chem. Soc.*, 2015, **137**, 8696–8699.

43 F. Zhang, W. Shi, J. Luo, N. Pellet, C. Yi, X. Li, X. Zhao, T. J. S. Dennis, X. Li, S. Wang, Y. Xiao, S. M. Zakeeruddin, D. Bi and M. Grätzel, *Adv. Mater.*, 2017, **29**, 1606806.

44 P. Docampo, F. C. Hanusch, S. D. Stranks, M. Döblinger, J. M. Feckl, M. Ehrensperger, N. K. Minar, M. B. Johnston, H. J. Snaith and T. Bein, *Adv. Energy Mater.*, 2014, **4**, 1400355.

45 W. Li, J. Fan, J. Li, Y. Mai and L. Wang, *J. Am. Chem. Soc.*, 2015, **137**, 10399–10405.

46 B. J. Foley, J. Girard, B. A. Sorenson, A. Z. Chen, J. Scott Niezgoda, M. R. Alpert, A. F. Harper, D.-M. Smilgies, P. Clancy, W. A. Saidi and J. J. Choi, *J. Mater. Chem. A*, 2017, **5**, 113–123.

47 P.-W. Liang, C.-Y. Liao, C.-C. Chueh, F. Zuo, S. T. Williams, X.-K. Xin, J. Lin and A. K. Y. Jen, *Adv. Mater.*, 2014, **26**, 3748–3754.

48 J. H. Heo, D. H. Song, H. J. Han, S. Y. Kim, J. H. Kim, D. Kim, H. W. Shin, T. K. Ahn, C. Wolf, T.-W. Lee and S. H. Im, *Adv. Mater.*, 2015, **27**, 3424–3430.

49 J. H. Heo, D. H. Song and S. H. Im, *Adv. Mater.*, 2014, **26**, 8179–8183.

50 N. J. Jeon, J. H. Noh, Y. C. Kim, W. S. Yang, S. Ryu and S. I. Seok, *Nat. Mater.*, 2014, **13**, 897–903.

51 M. Xiao, F. Huang, W. Huang, Y. Dkhissi, Y. Zhu, J. Etheridge, A. Gray-Weale, U. Bach, Y.-B. Cheng and L. Spiccia, *Angew. Chem., Int. Ed.*, 2014, **53**, 9898–9903.

52 J. Pascual, I. Kosta, E. Palacios-Lidon, A. Chuvilin, G. Grancini, M. K. Nazeeruddin, H. J. Grande, J. L. Delgado and R. Tena-Zaera, *J. Phys. Chem. C*, 2018, **122**, 2512–2520.

53 J. Burschka, N. Pellet, S.-J. Moon, R. Humphry-Baker, P. Gao, M. K. Nazeeruddin and M. Gratzel, *Nature*, 2013, **499**, 316–319.

54 J.-H. Im, I.-H. Jang, N. Pellet, M. Grätzel and N.-G. Park, *Nat. Nanotechnol.*, 2014, **9**, 927–932.

55 W. S. Yang, J. H. Noh, N. J. Jeon, Y. C. Kim, S. Ryu, J. Seo and S. I. Seok, *Science*, 2015, **348**, 1234–1237.

56 H. Zhang, J. Cheng, D. Li, F. Lin, J. Mao, C. Liang, A. K. Y. Jen, M. Grätzel and W. C. H. Choy, *Adv. Mater.*, 2017, **29**, 1604695.

57 Y. Wu, A. Islam, X. Yang, C. Qin, J. Liu, K. Zhang, W. Peng and L. Han, *Energy Environ. Sci.*, 2014, **7**, 2934–2938.

58 Q. Chen, H. Zhou, Z. Hong, S. Luo, H.-S. Duan, H.-H. Wang, Y. Liu, G. Li and Y. Yang, *J. Am. Chem. Soc.*, 2014, **136**, 622–625.

59 P. Docampo and T. Bein, *Acc. Chem. Res.*, 2016, **49**, 339–346.

60 J.-Y. Jeng, Y.-F. Chiang, M.-H. Lee, S.-R. Peng, T.-F. Guo, P. Chen and T.-C. Wen, *Adv. Mater.*, 2013, **25**, 3727–3732.

61 Y. Lin, B. Chen, F. Zhao, X. Zheng, Y. Deng, Y. Shao, Y. Fang, Y. Bai, C. Wang and J. Huang, *Adv. Mater.*, 2017, **29**, 1700607.

62 C. Tian, E. Castro, T. Wang, G. Betancourt-Solis, G. Rodriguez and L. Echegoyen, *ACS Appl. Mater. Interfaces*, 2016, **8**, 31426–31432.

63 C. Tian, K. Kochiss, E. Castro, G. Betancourt-Solis, H. Han and L. Echegoyen, *J. Mater. Chem. A*, 2017, **5**, 7326–7332.

64 Y. Xing, C. Sun, H. L. Yip, G. C. Bazan, F. Huang and Y. Cao, *Nano Energy*, 2016, **26**, 7–15.

65 Y. Zhao, W. Zhou, W. Ma, S. Meng, H. Li, J. Wei, R. Fu, K. Liu, D. Yu and Q. Zhao, *ACS Energy Lett.*, 2016, **1**, 266–272.

66 S. Erten-Ela, H. Chen, A. Kratzer, A. Hirsch and C. J. Brabec, *New J. Chem.*, 2016, **40**, 2829–2834.

67 J. Ha, H. Kim, H. Lee, K.-G. Lim, T.-W. Lee and S. Yoo, *Sol. Energy Mater. Sol. Cells*, 2017, **161**, 338–346.

68 J. H. Heo, H. J. Han, D. Kim, T. K. Ahn and S. H. Im, *Energy Environ. Sci.*, 2015, **8**, 1602–1608.

69 X. Liu, F. Lin, C.-C. Chueh, Q. Chen, T. Zhao, P.-W. Liang, Z. Zhu, Y. Sun and A. K. Y. Jen, *Nano Energy*, 2016, **30**, 417–425.

70 X. Meng, Y. Bai, S. Xiao, T. Zhang, C. Hu, Y. Yang, X. Zheng and S. Yang, *Nano Energy*, 2016, **30**, 341–346.

71 W. Qiu, J. P. Bastos, S. Dasgupta, T. Merckx, I. Cardinaletti, M. V. C. Jenart, C. B. Nielsen, R. Gehlhaar, J. Poortmans, P. Heremans, I. McCulloch and D. Cheyns, *J. Mater. Chem. A*, 2017, **5**, 2466–2472.

72 S. Shao, M. Abdu-Aguye, L. Qiu, L.-H. Lai, J. Liu, S. Adjokatse, F. Jahani, M. E. Kamminga, G. H. ten Brink, T. T. M. Palstra, B. J. Kooi, J. C. Hummelen and M. Antonietta Loi, *Energy Environ. Sci.*, 2016, **9**, 2444–2452.

73 Y. Shao, Z. Xiao, C. Bi, Y. Yuan and J. Huang, *Nat. Commun.*, 2014, **5**, 5784.

74 S. Chang, G. D. Han, J. G. Weis, H. Park, O. Hentz, Z. Zhao, T. M. Swager and S. Gradečak, *ACS Appl. Mater. Interfaces*, 2016, **8**, 8511–8519.

75 K. Wojciechowski, I. Ramirez, T. Gorisse, O. Dautel, R. Dasari, N. Sakai, J. M. Hardigree, S. Song, S. Marder, M. Riede, G. Wantz and H. J. Snaith, *ACS Energy Lett.*, 2016, **1**, 648–653.

76 T. Umeyama, D. Matano, S. Shibata, J. Baek, S. Ito and H. Imahori, *ECS J. Solid State Sci. Technol.*, 2017, **6**, M3078–M3083.

77 X. Liu, P. Huang, Q. Dong, Z. Wang, K. Zhang, H. Yu, M. Lei, Y. Zhou, B. Song and Y. Li, *Sci. China: Chem.*, 2017, **60**, 136–143.

78 Z. Kaicheng, Y. Hao, L. Xiaodong, D. Qingqing, W. Zhaowei, W. Yaofeng, C. Ning, Z. Yi and S. Bo, *Sci. China: Chem.*, 2017, **60**, 144.

79 Y. Li, Y. Zhao, Q. Chen, Y. Yang, Y. Liu, Z. Hong, Z. Liu, Y.-T. Hsieh, L. Meng and Y. Li, *J. Am. Chem. Soc.*, 2015, **137**, 15540–15547.

80 P.-W. Liang, C.-C. Chueh, S. T. Williams and A. K. Y. Jen, *Adv. Energy Mater.*, 2015, **5**, 1402321.

81 H. Azimi, T. Ameri, H. Zhang, Y. Hou, C. O. R. Quiroz, J. Min, M. Hu, Z.-G. Zhang, T. Przybilla, G. J. Matt, E. Spiecker, Y. Li and C. J. Brabec, *Adv. Energy Mater.*, 2015, **5**, 1401692.

82 X. Liu, W. Jiao, M. Lei, Y. Zhou, B. Song and Y. Li, *J. Mater. Chem. A*, 2015, **3**, 9278–9284.

83 C. Li, F. Wang, J. Xu, J. Yao, B. Zhang, C. Zhang, M. Xiao, S. Dai, Y. Li and Z. A. Tan, *Nanoscale*, 2015, **7**, 9771–9778.

84 Y. Bai, H. Yu, Z. Zhu, K. Jiang, T. Zhang, N. Zhao, S. Yang and H. Yan, *J. Mater. Chem. A*, 2015, **3**, 9098–9102.

85 K. Wojciechowski, S. D. Stranks, A. Abate, G. Sadoughi, A. Sadhanala, N. Kopidakis, G. Rumbles, C.-Z. Li, R. H. Friend, A. K. Y. Jen and H. J. Snaith, *ACS Nano*, 2014, **8**, 12701–12709.

86 W. Ke, D. Zhao, C. Xiao, C. Wang, A. J. Cimaroli, C. R. Grice, M. Yang, Z. Li, C.-S. Jiang, M. Al-Jassim, K. Zhu, M. G. Kanatzidis, G. Fang and Y. Yan, *J. Mater. Chem. A*, 2016, **4**, 14276–14283.

87 A. Abrusci, S. D. Stranks, P. Docampo, H.-L. Yip, A. K. Y. Jen and H. J. Snaith, *Nano Lett.*, 2013, **13**, 3124–3128.

88 C. Liu, K. Wang, P. Du, T. Meng, X. Yu, S. Z. D. Cheng and X. Gong, *ACS Appl. Mater. Interfaces*, 2015, **7**, 1153–1159.

89 K.-W. Tsai, C.-C. Chueh, S. T. Williams, T.-C. Wen and A. K. Y. Jen, *J. Mater. Chem. A*, 2015, **3**, 9128–9132.

90 C. M. Wolff, F. Zu, A. Paulke, L. P. Toro, N. Koch and D. Neher, *Adv. Mater.*, 2017, **29**, 1700159.

91 T. Cao, Z. Wang, Y. Xia, B. Song, Y. Zhou, N. Chen and Y. Li, *ACS Appl. Mater. Interfaces*, 2016, **8**, 18284–18291.

92 K. Wang, C. Liu, P. Du, J. Zheng and X. Gong, *Energy Environ. Sci.*, 2015, **8**, 1245–1255.

93 Y. Bai, Q. Dong, Y. Shao, Y. Deng, Q. Wang, L. Shen, D. Wang, W. Wei and J. Huang, *Nat. Commun.*, 2016, **7**, 12806.

94 Y.-H. Chao, Y.-Y. Huang, J.-Y. Chang, S.-H. Peng, W.-Y. Tu, Y.-J. Cheng, J. Hou and C.-S. Hsu, *J. Mater. Chem. A*, 2015, **3**, 20382–20388.

95 M. Valles-Pelarda, B. C. Hames, I. García-Benito, O. Almora, A. Molina-Ontoria, R. S. Sánchez, G. Garcia-Belmonte, N. Martín and I. Mora-Sero, *J. Phys. Chem. Lett.*, 2016, **7**, 4622–4628.

96 W. Zhou, J. Zhen, Q. Liu, Z. Fang, D. Li, P. Zhou, T. Chen and S. Yang, *J. Mater. Chem. A*, 2017, **5**, 1724–1733.

97 S. Chen, Y. Hou, H. Chen, M. Richter, F. Guo, S. Kahmann, X. Tang, T. Stubhan, H. Zhang, N. Li, N. Gasparini, C. O. R. Quiroz, L. S. Khanzada, G. J. Matt, A. Osvet and C. J. Brabec, *Adv. Energy Mater.*, 2016, **6**, 1600132.

98 Q. Xu, Z. Lu, L. Zhu, C. Kou, Y. Liu, C. Li, Q. Meng, W. Li and Z. Bo, *J. Mater. Chem. A*, 2016, **4**, 17649–17654.

99 M. Li, Y.-H. Chao, T. Kang, Z.-K. Wang, Y.-G. Yang, S.-L. Feng, Y. Hu, X.-Y. Gao, L.-S. Liao and C.-S. Hsu, *J. Mater. Chem. A*, 2016, **4**, 15088–15094.

100 J. Xie, X. Yu, J. Huang, X. Sun, Y. Zhang, Z. Yang, M. Lei, L. Xu, Z. Tang, C. Cui, P. Wang and D. Yang, *Adv. Sci.*, 2017, **4**, 1700018.

101 J. Xie, X. Yu, X. Sun, J. Huang, Y. Zhang, M. Lei, K. Huang, D. Xu, Z. Tang, C. Cui and D. Yang, *Nano Energy*, 2016, **28**, 330–337.

102 J. Peng, Y. Wu, W. Ye, D. A. Jacobs, H. Shen, X. Fu, Y. Wan, T. Duong, N. Wu, C. Barugkin, H. T. Nguyen, D. Zhong, J. Li, T. Lu, Y. Liu, M. N. Lockrey, K. J. Weber, K. R. Catchpole and T. P. White, *Energy Environ. Sci.*, 2017, **10**, 1792–1800.

103 C.-B. Tian, E. Castro, G. Betancourt-Solis, Z.-A. Nan, O. Fernandez-Delgado, S. Jankuru and L. Echegoyen, *New J. Chem.*, 2018, **42**, 2896–2902.

104 M. Shahiduzzaman, M. Karakawa, K. Yamamoto, T. Kusumi, K. Yonezawa, T. Kuwabara, K. Takahashi and T. Taima, *Sol. Energy Mater. Sol. Cells*, 2018, **178**, 1–7.

105 Y. Dong, W. Li, X. Zhang, Q. Xu, Q. Liu, C. Li and Z. Bo, *Small*, 2016, **12**, 1098–1104.

106 L. Gil-Escrig, C. Momblona, M. Sessolo and H. J. Bolink, *J. Mater. Chem. A*, 2016, **4**, 3667–3672.

107 L. Kegelmann, C. M. Wolff, C. Awino, F. Lang, E. L. Unger, L. Korte, T. Dittrich, D. Neher, B. Rech and S. Albrecht, *ACS Appl. Mater. Interfaces*, 2017, **9**, 17245–17255.

108 Q. Xue, Y. Bai, M. Liu, R. Xia, Z. Hu, Z. Chen, X.-F. Jiang, F. Huang, S. Yang, Y. Matsuo, H.-L. Yip and Y. Cao, *Adv. Energy Mater.*, 2017, **7**, 1602333.

109 X. Sun, L. Y. Ji, W. W. Chen, X. Guo, H. H. Wang, M. Lei, Q. Wang and Y. F. Li, *J. Mater. Chem. A*, 2017, **5**, 20720–20728.

110 J. Xu, A. Buin, A. H. Ip, W. Li, O. Voznyy, R. Comin, M. Yuan, S. Jeon, Z. Ning, J. J. McDowell, P. Kanjanaboos, J.-P. Sun, X. Lan, L. N. Quan, D. H. Kim, I. G. Hill, P. Maksymovych and E. H. Sargent, *Nat. Commun.*, 2015, **6**, 7081.

111 C.-H. Chiang and C.-G. Wu, *Nat. Photonics*, 2016, **10**, 196–200.

112 R. Sandoval-Torrientes, J. Pascual, I. García-Benito, S. Collavini, I. Kosta, R. Tena-Zaera, N. Martín and J. L. Delgado, *ChemSusChem*, 2017, **10**, 2023–2029.

113 Y. Wu, X. Yang, W. Chen, Y. Yue, M. Cai, F. Xie, E. Bi, A. Islam and L. Han, *Nat. Energy*, 2016, **1**, 16148.

114 S. Collavini, M. Saliba, W. Tress, P. Holzhey, S. Voelker, K. Domanski, S. Turren-Cruz, A. Ummadisingu, S. Zakeeruddin, A. Hagfeld, M. Graetzel and J. L. Delgado, *ChemSusChem*, 2017, DOI: 10.1002/cssc.201702265.

115 Y. Fang, C. Bi, D. Wang and J. Huang, *ACS Energy Lett.*, 2017, 782–794.

116 T. Heumueller, W. R. Mateker, A. Distler, U. F. Fritze, R. Cheacharoen, W. H. Nguyen, M. Biele, M. Salvador, M. von Delius, H.-J. Egelhaaf, M. D. McGehee and C. J. Brabec, *Energy Environ. Sci.*, 2016, **9**, 247–256.

117 H.-K. Lin, Y.-W. Su, H.-C. Chen, Y.-J. Huang and K.-H. Wei, *ACS Appl. Mater. Interfaces*, 2016, **8**, 24603–24611.

118 S. F. Volker, S. Collavini and J. L. Delgado, *ChemSusChem*, 2015, **8**, 3012–3028.

119 L. Meng, J. You, T.-F. Guo and Y. Yang, *Acc. Chem. Res.*, 2016, **49**, 155–165.

120 S.-M. Dai, X. Zhang, W.-Y. Chen, X. Li, Z. A. Tan, C. Li, L.-L. Deng, X.-X. Zhan, M.-S. Lin, Z. Xing, T. Wen, R.-M. Ho, S.-Y. Xie, R.-B. Huang and L.-S. Zheng, *J. Mater. Chem. A*, 2016, **4**, 18776–18782.

121 B. G. H. M. Groeneveld, M. Najafi, B. Steensma, S. Adjokatse, H.-H. Fang, F. Jahani, L. Qiu, G. H. T. Brink, J. C. Hummelen and M. A. Loi, *APL Mater.*, 2017, **5**, 076103.

122 S. Shao, J. Liu, H.-H. Fang, L. Qiu, G. H. ten Brink, J. C. Hummelen, L. J. A. Koster and M. A. Loi, *Adv. Energy Mater.*, 2017, 1701305.

123 J. Han, H.-Y. Wang, Y. Wang, M. Yu, S. Yuan, P. Sun, Y. Qin, Z.-X. Guo, J.-P. Zhang and X.-C. Ai, *RSC Adv.*, 2016, **6**, 112512–112519.

124 S.-M. Dai, L.-L. Deng, M.-L. Zhang, W.-Y. Chen, P. Zhu, X. Wang, C. Li, Z. A. Tan, S.-Y. Xie, R.-B. Huang and L.-S. Zheng, *Inorg. Chim. Acta*, 2017, **468**, 146–151.

125 E. Castro, G. Zavala, S. Seetharaman, F. D'Souza and L. Echegoyen, *J. Mater. Chem. A*, 2017, **5**, 19485–19490.

126 J. L. Delgado, E. Espíldora, M. Liedtke, A. Sperlich, D. Rauh, A. Baumann, C. Deibel, V. Dyakonov and N. Martín, *Chem. – Eur. J.*, 2009, **15**, 13474–13482.

127 J. Liu, X. Guo, Y. J. Qin, S. D. Liang, Z. X. Guo and Y. F. Li, *J. Mater. Chem.*, 2012, **22**, 1758–1761.

128 Q.-H. Zhang, W.-D. Hu, X.-F. Wang, G. Chen, J.-P. Zhang, L.-X. Xiao and T. Miyasaka, *Chem. Lett.*, 2017, **46**, 101–103.

129 C.-Y. Chang, W.-K. Huang, Y.-C. Chang, K.-T. Lee and C.-T. Chen, *J. Mater. Chem. A*, 2016, **4**, 640–648.

130 W. Xu, X. Yao, T. Meng, K. Wang, F. Huang, X. Gong and Y. Cao, *J. Mater. Chem. C*, 2017, **5**, 4190–4197.

131 C. Kuang, G. Tang, T. Jiu, H. Yang, H. Liu, B. Li, W. Luo, X. Li, W. Zhang, F. Lu, J. Fang and Y. Li, *Nano Lett.*, 2015, **15**, 2756–2762.

132 S. S. Kim, S. Bae and W. H. Jo, *Chem. Commun.*, 2015, **51**, 17413–17416.

133 G. Kakavelakis, T. Maksudov, D. Konios, I. Paradisanos, G. Kioseoglou, E. Stratakis and E. Kymakis, *Adv. Energy Mater.*, 2017, **7**, 1602120.

134 F. Xia, Q. Wu, P. Zhou, Y. Li, X. Chen, Q. Liu, J. Zhu, S. Dai, Y. Lu and S. Yang, *ACS Appl. Mater. Interfaces*, 2015, **7**, 13659–13665.

135 Y.-C. Wang, X. Li, L. Zhu, X. Liu, W. Zhang and J. Fang, *Adv. Energy Mater.*, 2017, **7**, 1701144.

136 C.-Z. Li, P.-W. Liang, D. B. Sulas, P. D. Nguyen, X. Li, D. S. Ginger, C. W. Schlenker and A. K. Y. Jen, *Mater. Horiz.*, 2015, **2**, 414–419.

137 H. J. Snaith, A. Abate, J. M. Ball, G. E. Eperon, T. Leijtens, N. K. Noel, S. D. Stranks, J. T. Wang, K. Wojciechowski and W. Zhang, *J. Phys. Chem. Lett.*, 2014, **5**, 1511–1515.

138 C. Tao, S. Neutzner, L. Colella, S. Marras, A. R. Srimath Kandada, M. Gandini, M. D. Bastiani, G. Pace, L. Manna, M. Caironi, C. Bertarelli and A. Petrozza, *Energy Environ. Sci.*, 2015, **8**, 2365–2370.

139 J. Will, Y. Hou, S. Scheiner, U. Pinkert, I. M. Hermes, S. A. L. Weber, A. Hirsch, M. Halik, C. Brabec and T. Unruh, *ACS Appl. Mater. Interfaces*, 2018, **10**, 5511–5518.

140 Q. Wang, Y. Shao, Q. Dong, Z. Xiao, Y. Yuan and J. Huang, *Energy Environ. Sci.*, 2014, **7**, 2359–2365.

141 J. Pascual, I. Kosta, T. Tuyen Ngo, A. Chuvilin, G. Cabanero, H. J. Grande, E. M. Barea, I. Mora-Seró, J. L. Delgado and R. Tena-Zaera, *ChemSusChem*, 2016, **9**, 2679–2685.

142 C. Liu, K. Wang, P. Du, C. Yi, T. Meng and X. Gong, *Adv. Energy Mater.*, 2015, **5**, 1402024.

143 C. Liu, W. Li, H. Li, C. Zhang, J. Fan and Y. Mai, *Nanoscale*, 2017, **9**, 13967–13975.

144 C. Park, H. Ko, D. H. Sin, K. C. Song and K. Cho, *Adv. Funct. Mater.*, 2017, **27**, 1703546.

145 T. M. Khan, Y. Zhou, A. Dindar, J. W. Shim, C. Fuentes-Hernandez and B. Kippelen, *ACS Appl. Mater. Interfaces*, 2014, **6**, 6202–6207.

146 S.-H. Liao, Y.-L. Li, T.-H. Jen, Y.-S. Cheng and S.-A. Chen, *J. Am. Chem. Soc.*, 2012, **134**, 14271–14274.

147 J. Seo, S. Park, Y. Chan Kim, N. J. Jeon, J. H. Noh, S. C. Yoon and S. I. Seok, *Energy Environ. Sci.*, 2014, **7**, 2642–2646.

148 S. Bai, Z. Wu, X. Wu, Y. Jin, N. Zhao, Z. Chen, Q. Mei, X. Wang, Z. Ye, T. Song, R. Liu, S.-T. Lee and B. Sun, *Nano Res.*, 2014, **7**, 1749–1758.

149 P. Docampo, J. M. Ball, M. Darwich, G. E. Eperon and H. J. Snaith, *Nat. Commun.*, 2013, **4**, 2761.

150 C.-Z. Li, C.-C. Chueh, H.-L. Yip, F. Ding, X. Li and A. K. Y. Jen, *Adv. Mater.*, 2013, **25**, 2457–2461.

151 Y. Liu, M. Bag, L. A. Renna, Z. A. Page, P. Kim, T. Emrick, D. Venkataraman and T. P. Russell, *Adv. Energy Mater.*, 2016, **6**, 1501606.

152 C. Cui, Y. Li and Y. Li, *Adv. Energy Mater.*, 2017, **7**, 1601251.

153 J. Xie, X. Yu, J. Huang, X. Sun, Y. Zhang, Z. Yang, M. Lei, L. Xu, Z. Tang, C. Cui, P. Wang and D. Yang, *Adv. Sci.*, 2017, **4**, 1700018.

154 M. Li, Z.-K. Wang, T. Kang, Y. Yang, X. Gao, C.-S. Hsu, Y. Li and L.-S. Liao, *Nano Energy*, 2018, **43**, 47–54.

155 Z. Zhu, C.-C. Chueh, F. Lin and A. K. Y. Jen, *Adv. Sci.*, 2016, **3**, 1600027.

156 B. L. Watson, N. Rolston, K. A. Bush, T. Leijtens, M. D. McGehee and R. H. Dauskardt, *ACS Appl. Mater. Interfaces*, 2016, **8**, 25896–25904.

157 J. Yin, D. Cortecchia, A. Krishna, S. Chen, N. Mathews, A. C. Grimsdale and C. Soci, *J. Phys. Chem. Lett.*, 2015, **6**, 1396–1402.

158 C. Quarti, F. De Angelis and D. Beljonne, *Chem. Mater.*, 2017, **29**, 958–968.

159 M. F. N. Taufique, S. M. Mortuza and S. Banerjee, *J. Phys. Chem. C*, 2016, **120**, 22426–22432.

160 J. Yang, B. D. Siempelkamp, D. Liu and T. L. Kelly, *ACS Nano*, 2015, **9**, 1955–1963.

161 J. A. Christians, P. A. M. Herrera and P. V. Kamat, *J. Am. Chem. Soc.*, 2015, **137**, 1530–1538.

162 J. Yang and T. L. Kelly, *Inorg. Chem.*, 2017, **56**, 92–101.

163 A. M. A. Leguy, Y. Hu, M. Campoy-Quiles, M. I. Alonso, O. J. Weber, P. Azarhoosh, M. van Schilfgaarde, M. T. Weller, T. Bein, J. Nelson, P. Docampo and P. R. F. Barnes, *Chem. Mater.*, 2015, **27**, 3397–3407.

164 M. I. Asghar, J. Zhang, H. Wang and P. D. Lund, *Renewable Sustainable Energy Rev.*, 2017, **77**, 131–146.

165 Q. Jiang, D. Rebollar, J. Gong, E. L. Piacentino, C. Zheng and T. Xu, *Angew. Chem., Int. Ed.*, 2015, **54**, 7617–7620.

166 Q. Tai, P. You, H. Sang, Z. Liu, C. Hu, H. L. W. Chan and F. Yan, *Nat. Commun.*, 2016, **7**, 11105.

167 H.-S. Kim, C.-R. Lee, J.-H. Im, K.-B. Lee, T. Moehl, A. Marchioro, S.-J. Moon, R. Humphry-Baker, J.-H. Yum, J. E. Moser, M. Grätzel and N.-G. Park, *Sci. Rep.*, 2012, **2**, 591.

168 R. K. Misra, S. Aharon, B. Li, D. Mogilyansky, I. Visoly-Fisher, L. Etgar and E. A. Katz, *J. Phys. Chem. Lett.*, 2015, **6**, 326–330.

169 F. T. F. O'Mahony, Y. H. Lee, C. Jellett, S. Dmitrov, D. T. J. Bryant, J. R. Durrant, B. C. O'Regan, M. Graetzel, M. K. Nazeeruddin and S. A. Haque, *J. Mater. Chem. A*, 2015, **3**, 7219–7223.

170 N. Aristidou, I. Sanchez-Molina, T. Chotchuangchutchaval, M. Brown, L. Martinez, T. Rath and S. A. Haque, *Angew. Chem., Int. Ed.*, 2015, **54**, 8208–8212.

171 D. Bryant, N. Aristidou, S. Pont, I. Sanchez-Molina, T. Chotchunangatchaval, S. Wheeler, J. R. Durrant and S. A. Haque, *Energy Environ. Sci.*, 2016, **9**, 1655–1660.

172 A. Dualeh, P. Gao, S. I. Seok, M. K. Nazeeruddin and M. Grätzel, *Chem. Mater.*, 2014, **26**, 6160–6164.

173 P. Pistor, J. Borchert, W. Fränzel, R. Csuk and R. Scheer, *J. Phys. Chem. Lett.*, 2014, **5**, 3308–3312.

174 T. Supasai, N. Rujisamphan, K. Ullrich, A. Chemseddine and T. Dittrich, *Appl. Phys. Lett.*, 2013, **103**, 183906.

175 J. Yang, B. D. Siempelkamp, E. Mosconi, F. De Angelis and T. L. Kelly, *Chem. Mater.*, 2015, **27**, 4229–4236.

176 D. Liu, J. Yang and T. L. Kelly, *J. Am. Chem. Soc.*, 2014, **136**, 17116–17122.

177 Q. Hu, J. Wu, C. Jiang, T. Liu, X. Que, R. Zhu and Q. Gong, *ACS Nano*, 2014, **8**, 10161–10167.

178 Y. Cheng, Q.-D. Yang, J. Xiao, Q. Xue, H.-W. Li, Z. Guan, H.-L. Yip and S.-W. Tsang, *ACS Appl. Mater. Interfaces*, 2015, **7**, 19986–19993.

179 B. Philippe, B.-W. Park, R. Lindblad, J. Oscarsson, S. Ahmadi, E. M. J. Johansson and H. Rensmo, *Chem. Mater.*, 2015, **27**, 1720–1731.

180 B. Conings, J. Drijkoningen, N. Gauquelin, A. Babayigit, J. D'Haen, L. D'Olieslaeger, A. Ethirajan, J. Verbeeck, J. Manca, E. Mosconi, F. D. Angelis and H.-G. Boyen, *Adv. Energy Mater.*, 2015, **5**, 1500477.

181 N. Aristidou, C. Eames, I. Sanchez-Molina, X. Bu, J. Kosco, M. S. Islam and S. A. Haque, *Nat. Commun.*, 2017, **8**, 15218.

182 L. Zheng, Q. Zhou, X. Deng, M. Yuan, G. Yu and Y. Cao, *J. Phys. Chem. B*, 2004, **108**, 11921–11926.

183 Y. Fang, C. Bi, D. Wang and J. Huang, *ACS Energy Lett.*, 2017, **2**, 782–794.

184 N. K. Noel, A. Abate, S. D. Stranks, E. S. Parrott, V. M. Burlakov, A. Goriely and H. J. Snaith, *ACS Nano*, 2014, **8**, 9815–9821.

185 Y.-S. Jung, K. Hwang, F. H. Scholes, S. E. Watkins, D.-Y. Kim and D. Vak, *Sci. Rep.*, 2016, **6**, 20357.

186 M. A. Green, K. Emery, Y. Hishikawa, W. Warta, E. D. Dunlop, D. H. Levi and A. W. Y. Ho-Baillie, *Prog. Photovolt.: Res. Appl.*, 2017, **25**, 3–13.

187 S. Senthilarasu, E. F. Fernández, F. Almonacid and T. K. Mallick, *Sol. Energy Mater. Sol. Cells*, 2015, **133**, 92–98.

188 M. Salado, M. A. Fernández, J. P. Holgado, S. Kazim, M. K. Nazeeruddin, P. J. Dyson and S. Ahmad, *ChemSusChem*, 2017, **10**, 3846–3853.

189 W. Li, C. Zhang, Y. Ma, C. Liu, J. Fan, Y. Mai and R. E. I. Schropp, *Energy Environ. Sci.*, 2018, **11**, 286–293.

190 A. F. Akbulatov, L. A. Frolova, M. P. Griffin, I. R. Gearba, A. Dolocan, D. A. Vanden Bout, S. Tsarev, E. A. Katz, A. F. Shestakov, K. J. Stevenson and P. A. Troshin, *Adv. Energy Mater.*, 2017, **7**, 1700476.

191 Y. Han, S. Meyer, Y. Dkhissi, K. Weber, J. M. Pringle, U. Bach, L. Spiccia and Y.-B. Cheng, *J. Mater. Chem. A*, 2015, **3**, 8139–8147.

192 Y. S. Kwon, J. Lim, H.-J. Yun, Y.-H. Kim and T. Park, *Energy Environ. Sci.*, 2014, **7**, 1454–1460.